INVESTIGATION OF ACOUSTIC EMISSION IN TISSUE DEFORMATION

Jason Law

201492893

Thesis submitted towards the partial fulfilment of

MSc Biomedical Engineering

2014/2015

Supervised by

Dr Arjan Buis

University of Strathclyde

Department of Biomedical Engineering

DECLARATION

This thesis is the result of the author's original research. It has been composed by the author and has not been previously submitted for examination which has led to the award of a degree.

Signed:_____

Date:_____

ACKNOWLEDGEMENTS

The completion of this project was only possible with the help and support of several people.

Firstly I would like to take this opportunity to thank my supervisor Dr Arjan Buis for his guidance, time and support especially when the obstacles seemed neverending and providing another viewpoint to the challenges.

I am also grateful for Dr Francesco Guarato in his assistance, with MatLab, and provision of acoustic recording equipment which allowed this project to move forward.

I am also thankful for Dr Phil Riches patiently answering my questions, training and guiding me in using the Bose machine.

Finally I would like to thank my friends and family for their support throughout this year.

ABSTRACT

Following amputation there is a risk of deep tissue injury when mobilising with a prosthesis which occurs due to dynamic deformation of soft tissue between the skeleton and the prosthetic socket. Current detection methods are invasive, cumbersome and do not provide real-time information. If shear stress is considered then it can ultimately be defined as fibres being pulled apart such as a fabric being torn. As such an acoustic noise maybe emitted and potentially quantifiable in real-time.

The aim is to conduct exploratory experiments determining whether acoustic emission during tissue deformation is detectable for future influence of socket design.

Animal tissue were prepared from two pork *psoas major* muscles into transverse and longitudinal specimens. A series of pilot studies were performed applying uniaxial displacement controlled tensile loads at a rate of 1mm/s using a Bose testing machine. These loads applied either 7mm or 9mm maximum displacement on differing specimen lengths to explore the optimum protocol. Specimens were submerged in either a temperature controlled or non-controlled water bath. Simultaneous acoustic recording took place using a hydrophone and digital oscilloscope along with stress and strain data from the Bose machine.

Only the transverse specimens fractured and a signal seemed present on the oscilloscope display but due to Bose machine noise no quantifiable frequencies were discovered. Longitudinal specimens required more displacement than feasible to fracture.

In conclusion these results are unable to determine if acoustic emission are detectable during tissue deformation. To provide more conclusive evidence either more sensitive, quieter instruments needs development or larger specimens with greater displacement are required.

CONTENTS

LIST OF FIGURES

1 BACKGROUND

1.1 Deep Tissue Injury

Pressure ulcers can be broadly classed into two groups, superficial and deep [1, 2]. Superficial ulcers develops from the epidermal skin layer [3, 4]. The mechanisms that contribute to superficial pressure ulcer development include moisture and heat combined with frictional and shear forces, infection, poor nutrition and impaired skin sensation [2-4]. Generally superficial pressure ulcers are reversible since these wounds are confined to the top layer of skin [2]. Deep pressure ulcers (DPU) have a very different mechanism [2] and along with deep tissue injury (DTI) tends to occur around a bony prominence below intact skin [5-7]. Both DPU and DTI arises from prolonged application of pressure or compressive forces, which can be due to immobility in bed/wheelchair bound patients or potentially prolonged use of orthoses or prostheses [6, 8].

The term DTI was used to describe a pressure ulcer that is likely to have high pressure at the bone-muscle interface [9]. DTI differs due to the erosion of soft tissues near the bony prominence, usually muscle, that occurs first then subsequent subcutaneous soft tissue layers such as fat and skin [2, 9]. As the muscle disintegrates this leads to increased stiffness therefore increasing the stresses on adjacent tissue such as the superficial layer [2, 3, 10]. This in turn increases the amount of tissue necrosis leading to a positive-feedback cycle which may continue until the lesion breaks through the epidermal layer [2, 3, 10]

DTI may be detected late as they present with the only external appearance of a deep bruise (Figure 1.1) and can be misdiagnosed as a superficial pressure ulcer [11, 12]. It is also problematic that most amputations occur due to vascular diseases [13] which are often associated with a level of peripheral neuropathy [14]. This along with the poor adaptation of skin and underlying soft tissues to high loads [15] places the residual limb at increased risk of DTI due to a lack of sensorial feedback. If no action is taken, there is a risk of further debridement and amputation due to increasing tissue necrosis.

Figure 1.1 External appearance of suspected DTI and affected layers

On the left shows a typical picture of suspected DTI, which looks like a bruise and on the right the layers of tissue affected [1]

Currently there are a number of theories relating to the cause of DTI, which include pressure-related ischaemia, reperfusion injuries due to blood rushing back to ischaemic tissues upon unloading and recently tissue deformation and ischaemia related deformation injuries [5, 16-18]. There has been research displaying a causal relationship between localised deformation and tissue damage. In the same study it showed that the tissue damage increases with strain [16]. Also it has been shown that two hours of tissue compression leads to permanent muscle damage whilst ischaemia is reversible [6, 17]. Portnoy et al (2008) investigated the internal mechanical condition of a trans-tibial residual limb during static weight bearing and found that the magnitude of tensile and shear strain within the tissues were much greater than the compressive strain values. This provides further support that tension and shear

are of greater significance in the initiation of DTI [18]. High internal shear could also develop in tissue compression [19]. Hence DTI detection could be used to assess the biomechanical fit of a prosthetic socket using tissue deformation as a measurement parameter [20].

1.1.1 Role of Shear in DTI

Shear forces can be separated into internal and external categories. Shear can develop when external frictional forces stretches the top layer of skin as it slides against a supporting surface such as bone or against a prosthetic socket as shown in Figure 1.2 [21, 22]. This same concept of two different surfaces can be applied to internal tissue shear where subcutaneous tissue and muscle slide over one another.

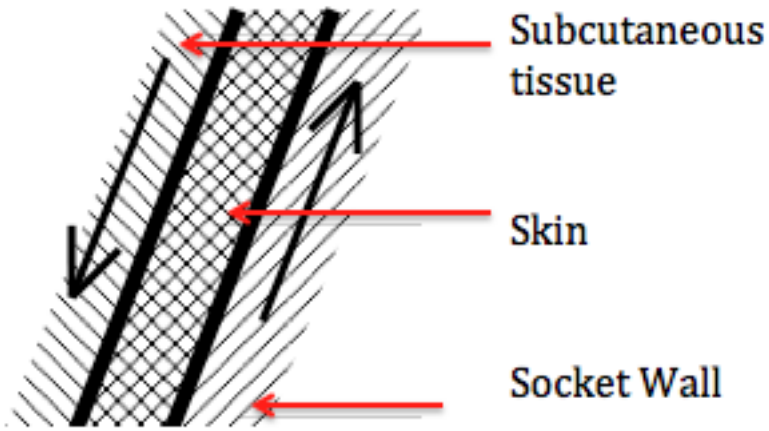

Figure 1.2 Development of external shear forces in soft tissue

These can develop when two surfaces slide in opposite direction. Adapted from Klasson et al, 2006 [19]

Both external frictional forces and internal tissue shear contribute to pressure ulcer formation but these two forces are more significant in DTI [21]. Both of these forces interact for example internal shear will increase around the bony prominences where the skin has been stretched. This type of shear is commonly seen in pressure ulcer formation especially around the sacrum however this can occur on any part of the body even in a cast. In a case study, Farid et al [23], stressed the neutral position of the foot (perpendicular to the leg) while a walking cast was applied. They applied this to avoid 'pistoning', or the residual limb slipping up and down in the socket whilst walking, with each step due to the downward angle of the foot. If pistoning

occurred then the soft tissues of the foot would shear. This can also be applied to the coupling or interface between the skeleton of an amputee and prosthetic socket wall.

The most sensitive tissue to shear is muscle due to the longitudinal layering of cells and muscle fibre bundles which are enveloped together by connective tissue (Figure 1.3), which has different stiffness to muscle fibre bundles [3, 21].

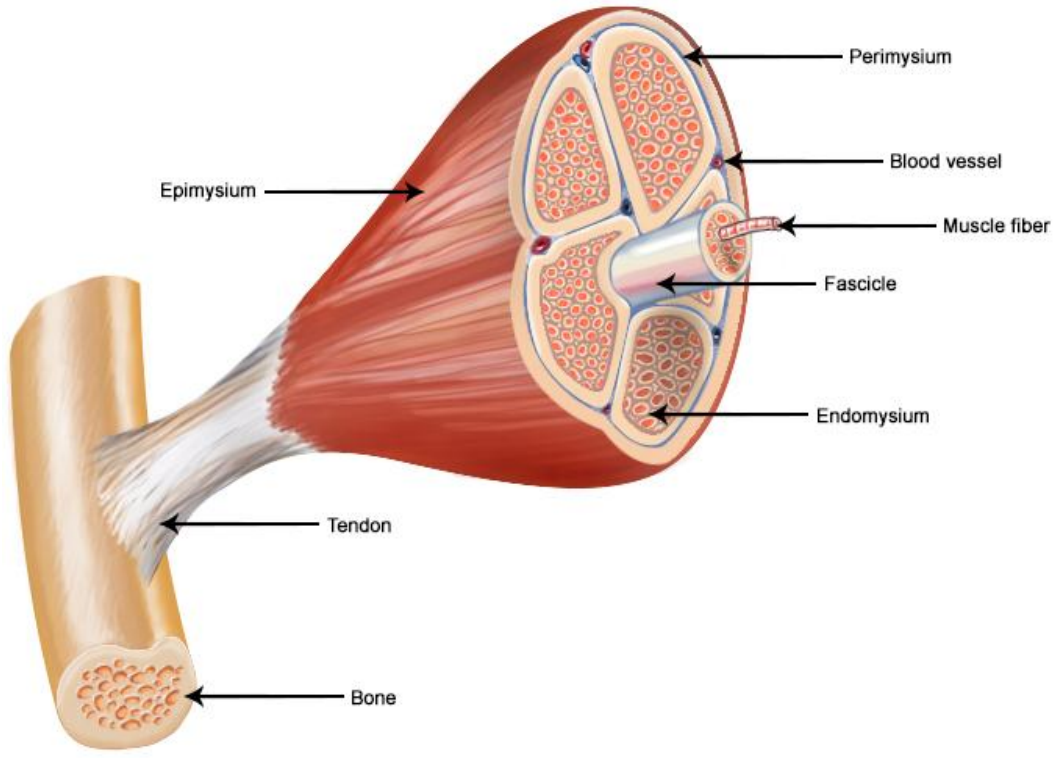

Figure 1.3 Skeletal Muscle Structure

The hierarchal organisation of skeletal muscle is displayed. The epimysium, perimysium and endomysium are all connective tissue that encompasses the different layers of muscle fibres and fascicles [24]

Hence these muscle fibre bundles slides over each other whilst weight bearing. If muscle shears then cells are damaged leading to muscle destruction or rhabdomyolysis [21].

1.2 Review of Current Methods of Detecting DTI

1.2.1 Chemistry

1.2.1a Urine

As DTI involves skeletal muscle then a common complication is rhabdomyolysis [21, 25-27]. This results in the release of myoglobulins into the bloodstream due to the shear forces on muscle. The myoglobulins are filtered through the renal glomeruli resulting in amber or brown coloured urine thus enabling detection through urinalysis or urine dipstick [21]. However a review [28] of the literature reveals that the half-life for myoglobulins in urine is approximately 4-6 hours thus the discolouration may be missed.

1.2.1b Blood

Another quantifiable measure of rhabdomyolysis is the release of creatine phosphokinase (CK) in the blood stream, which is an enzyme specific to muscle tissue. Normal levels are between 60-400 IU/L however when levels are elevated greater than 1000 IU/L some muscle destruction can be assumed. CK levels tend to rise in the first 12 hours of muscle destruction, peaking between 12 – 72 hours then declining post 72 hours of muscle death. Elevated CK and myoglobulinuria (presence of myoglobulins in urine) are possible indications of DTI despite a lack of visible skin changes [21]. Though elevated CK levels may be due to other reasons such as heart attacks or cerebrovascular accidents. Two literature reviews [17, 29] suggest that DTI may be present on admission providing no other muscle injuries present. This occurs where the presence of DTI occurs within one week of hospital admission following an elevated CK in the first 24 hours of admission. Clearly a major limitation with use of myoglobulinuria and CK are that they provide delayed not real-time information.

1.2.2 Sonography

Another method of DTI detection is the use of ultrasound or sonography. It provides a hands-on real time examination that allows structures to be viewed whilst

interacting with the patient. Another advantage is the speed of examination and portability depending on anatomic structures studied [21, 30].

1.2.2a Generation of Ultrasound Image

The equipment consists of the ultrasound machine and probe. In a scan the probe (Figure 1.4) emits sonic impulses, via a piezoelectric crystal, and reflections are transmitted back to the probe, which then converts these reflections into images.

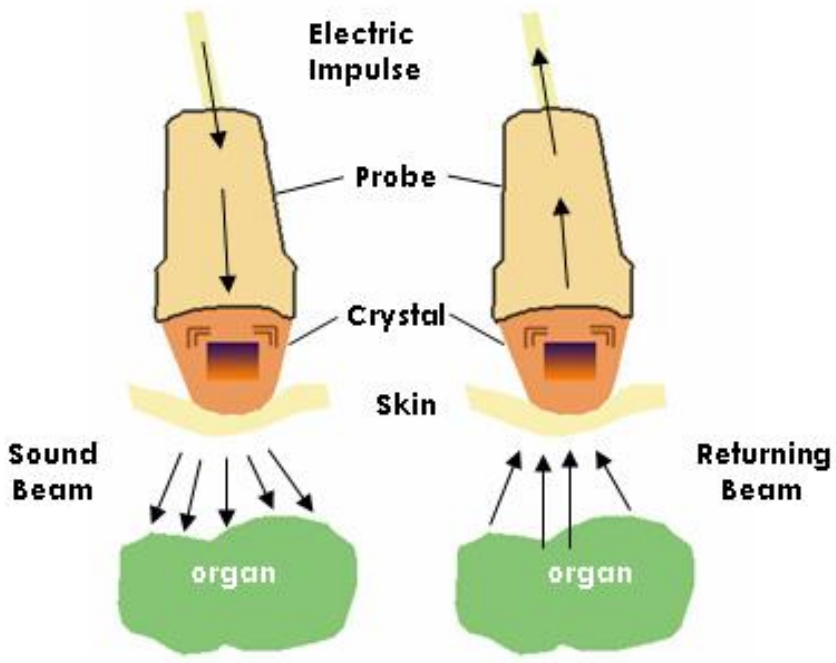

Figure 1.4 A schematic diagram for a medical ultrasound probe
From Ultrasound for Regional Anaesthesia [31]

These images are comprised of shades ranging from black (no reflections) to white (strong reflections) [21]. Different tissues, such as fascia, muscle tendons and bone will reflect these impulses to varying degrees producing detailed images. Subtle abnormalities within these tissues can also be detected thus providing potential in DTI detection especially as sonography is an excellent imaging modality for the musculoskeletal system [32].

1.2.2b Suitability for Detecting Tissue Death

One of the first signs of muscle death, that was identified in animal studies is 'stiffening' compared to other normal tissues [3]. Due to the sensitivity of ultrasound

to changes in tissue consistency this sign was detectable in a prospective study by Deprez et al [33]. This study used numerical simulations and physical acquisitions on pressure ulcer mimicking phantoms and in vivo experiments on rats and further corroborated the potential for ultrasound in detecting early pressure ulcer formation when no visible signs are present.

There are a number of animal and forensic studies which suggest significant changes occur 7 days post injury causing DTI to become visible [34-38]. However different terminology and descriptive terms are used regarding the development of DTI in these studies. For future research investigators will need to agree on these terms at various time point to correlate and provide clarity on the subject [21].

1.2.2c Clinical Practice

In clinical practice ultrasound has been used to detect early signs of rhabdomyolysis where the patients' symptoms occurred within 24 hours of the examination [39]. Though this is not DTI, it highlights the sensitivity of ultrasound in muscle injury detection [21]. Sonography has been used to successfully exclude DTI when evaluating a diabetic patient's heel which was red [21]. The investigators found that sonography was sensitive to tissue substructural changes i.e. abnormal oedema between the dermis and subcutaneous layers. These changes signify the early damage due to friction and shear thus supporting sonography's potential in DTI detection. Upon follow up examination the patient's heel made full recovery after 2 weeks pressure relief [21].

Aoi et al commented that there have been few reports on the characteristic DTI ultrasonic findings and their relationship with clinical manifestations and prognosis [40]. They went on to report a set of four characteristics but this has yet to be widely accepted.

However even if DTI characteristics were widely accepted, attachment of the ultrasonic transducer can prove to be troublesome with prosthetic sockets. Murray and Convery [41] analysed the motion of the residual femur within a trans-femoral socket during gait. They describe a time consuming process of creating multiple sockets and ensuring optimal positions are acquired before finally creating holes within the socket wall for transducer attachment.

1.2.2d Summary

In general ultrasound technology does have the potential to easily detect DTI at a patient's bedside however further research is required upon agreement of ultrasonic findings as well as corresponding terminology with DTI chronological stages. Though once agreement has been reached, incorporation into prosthetic socket design may prove impractical.

1.2.3 Magnetic Resonance Imaging (MRI)

1.2.3a Generation of an MRI image

There has been some research examining muscle DTI and MRI. Before a discussion of DTI and MRI can occur an understanding of how MRI images are generated is required.

MRI requires a strong oscillating magnetic field to disrupt protons (a hydrogen nucleus), found abundantly in water and fat. Normally these protons with in the body will have their axes randomly aligned. However when placed in a strong magnetic field these protons will line up which creates a magnetic vector along the axis of the MRI scanner. These protons are then further disrupted by radio wave energy deflecting the magnetic vector by multiple radiofrequency pulses. Once these pulses cease the time for the protons to fully relax can be measured in two ways. The first is called T1 (spin-lattice or longitudinal), which is the time for the magnetic vector to return to its resting state. The second measures the time for axial spin to return to its resting state and is called T2 (spin-spin or transverse) [42].

1.2.3b T2 Imaging

Stekelenburg et al [6] performed in vivo uniaxial indentor compression and ischaemic loading, via inflatable tourniquet, experiments on the tibialis anterior of rats. They then analysed the damage using T2 weighted and contrast enhanced MRI imaging with histology.

Changes in transverse relaxation (T2) are generally accepted as a measure of tissue damage [43]. Pressure Ulcers tend to be associated with inflammation, oedema, necrosis haemorrhage, fibrosis and fatty infiltration, which also affect muscle proton density and relaxation times. Three of these pathological features,

oedema inflammation and haemorrhage, are caused by increased intra- and extracellular free water. This result in increased T1 and T2 as free water has longer relaxation times [6]. T1 though is relatively insensitive to muscle state changes but maps the structural aspects. In contrast T2 is highly sensitive to tissue changes hence the rationale for this type of scanning in Stekelenburg et al study [6]. They found an increased signal intensity extending from the skin to the bone on T2 weighted images, which were corroborated with their contrast enhanced scans. They also found marked difference after two hours of pure ischaemic loading and compression testing. On T2 images there were increased signal in regions that correlated to necrosis and muscle fibre damage. However with pure ischaemic loading they found the changes returned to normal within 40 minutes. [6]

1.2.3c Diffusion Tensor Imaging

In another study Van Nierop et al [44] aimed to investigate the effect of small molecule diffusion, such as oxygen and carbon dioxide, during deformation. They used water diffusion as a surrogate for these molecules and performed similar compression indentor tests to Stekelenburg et al [6] using T2 and diffusion tensor

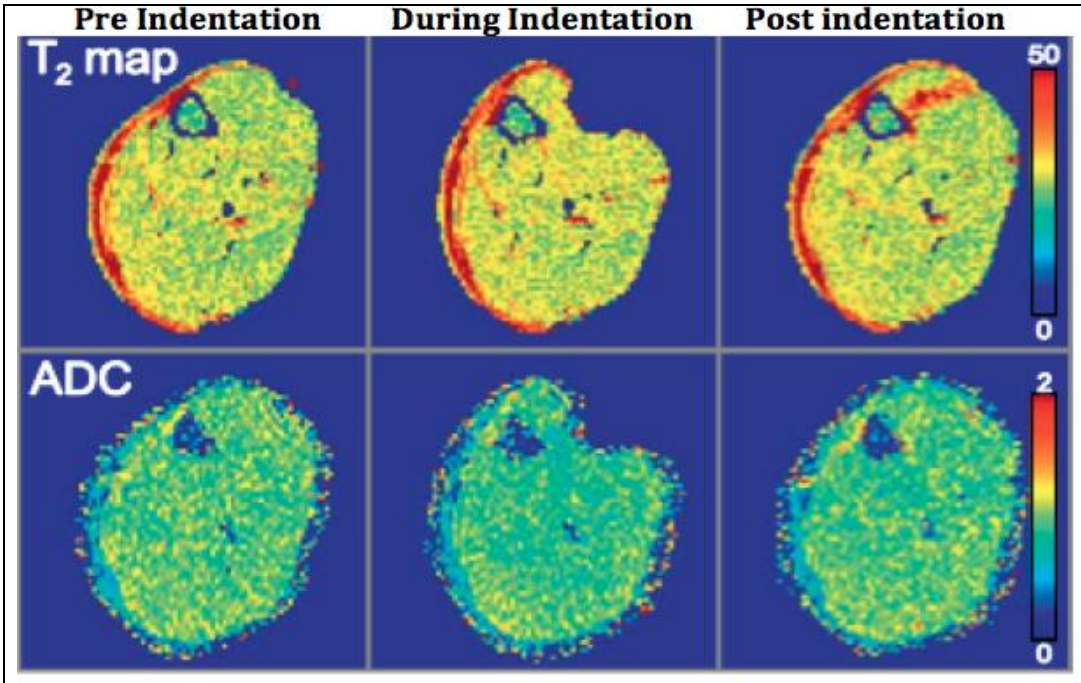

Figure 1.5 Typical T2 and diffusion tensor images during indentation

T2 images are on the top row and diffusion tensor on the bottom row. From van Nierop et al [44]

imaging.

Diffusion tensor imaging is a form of MRI that measures water diffusion. It has primarily been of great use in the field of neurology and neuroscience. The brain is comprised of microscopically organised myelinated axons in certain directions within the white matter. Diffusion tensor imaging is sensitive to these directional constraints, by measuring the apparent diffusion coeffiecient (ADC), and is clinically useful in early detection of ischaemic strokes. Diffusion tensor imaging can also be applied to other tissues that are directionally organised such as muscle [45].

Van Nierop et al [44] found that though ADC decreased during deformation this normalised post indentation as seen in Figure 1.5. They also found increased T2 signal intensity post indentation which agreed with data from Stekelenburg et al [6]. When comparing corresponding T2 and ADC values Van Nierop et al found no statistical difference implying that water diffusion was not affected by tissue deformation [44].

1.2.3d Summary

In general MRI can detect DTI notably using T2 though not diffusion tensor imaging. However MRI is an expensive, time consuming process and can be exclusive of patients with magnetic sensitive implants.

1.2.4 Summary of Current Detection Methods

There are several methods to infer and detect the onset of DTI all of which have current clinical use and a body of supporting research. However they prove to be invasive (serum chemistry), provide latent information i.e not real time (urine and serum chemistry along with MRI), expensive (MRI) or require specialist knowledge to interpret (sonography and MRI). Currently sonography seems most promising in DTI detection due to the portability and economical factors however further research is required to define the specific characteristics. Another viewpoint may be to analyse acoustic emission arising from shear stress.

1.3 Acoustic Emission and Tissue Fibres

Acoustic emission (AE) is a phenomenon which occurs when a material is placed under stress then a sudden release of strain energy creates a sound wave due to the relative movement between atomic chains. The event signifies degradation of the internal structure and has been used to detect material fatigue [46, 47]. The benefits of this method are non-invasive and non-destructive [48-50] requiring no input signal as the acoustic waves are generated by the material. This allows transducers to be placed anywhere on the materials' surface to monitor acoustic output a nd provides a method of assessing the internal structure of a material [48]. However AE signals tend to be weak and may be affected by background noise from the environment as well as propagation through the material; therefore more advanced microphones may be required to capture the signals [49-51]. Another advantage of AE testing is the ability to assess the integrity of a material whilst in operation thus data can be retrieved in real-time therefore acting as an early warning system [48, 51].

Sound waves are released as muscle contracts which can then be detected by using acoustic myography (AMG), a specialised AE technique [52-56]. Interestingly the contractile force is proportional to the volume of the acoustic noise [52, 53]. Also it is thought that the noise arises from the lateral oscillations of fibres [52, 56, 57]. This signal has been utilised, by adapting AMG, to analyse muscle activity and fatigue [52, 54, 56, 57] and to control an externally powered upper limb prosthesis [55]. The movement which occurs within muscle tissue during deformation could potentially release AE wave as atomic dislocations produces pressure waves travelling through the tissue and detectable on the surface [51]. Since tendons and skeletal muscles are known to be composed of uni-directional fibres, when these tissues are loaded in a multi-directionally they have the potential to develop shear stresses [58] that can be detected by AE.

Previous work [51] have investigated whether AE exists during tensile testing of a single porcine intercostal muscle, with bones still attached, and three lower chicken legs again with bony attachment. The bones were utilised as a clamping point to minimise slippage. These experiments were performed using a hydrophone and Instron testing machine. Only the pork and one chicken specimen failed by muscle detachment at the bone. No acoustic signal was detected. The other two chicken specimens slipped or did not fail. It seemed that by utilising bone as gripping points this prevented muscle rupture as the weakest point are the muscle insertion onto bone. Other limitations with this work are that the Instron machine is normally used for large industrial material testing and may not be suitable for applying smaller and more sensitive loads to small biological specimens. The author also raised the question as to whether the hydrophone was sensitive enough to detect the AE resulting from shear stress and suggested the use of contact microphone.

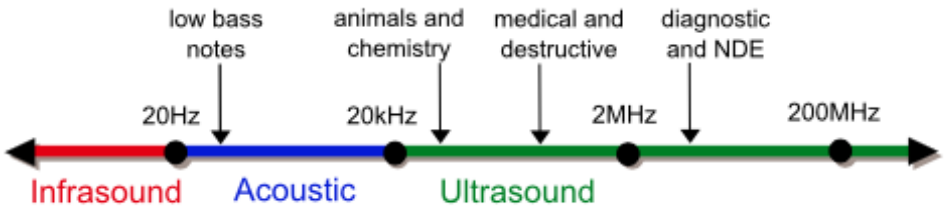

Figure 1.6 Operational frequency range of acoustic applications in blue and theorised range of signal

Adapted from Buis et al [59]

Since this is novel work it has been theorised that the frequency range of the acoustic signal will be 20Hz- 20kHz, see Figure 1.6 [59].

1.4 Context

It has been quoted as high as 90% that vascular disease is the major causal factor for lower limb amputations in the UK [60] of which 60% of cases are due to atherosclerosis and 30% due to diabetes mellitus. The majority of these amputations are likely to be trans-tibial to provide patients with minimal ambulatory difficulties. Due to the associated neuropathy with dysvascularity this places the residual limb at risk of DTI which will negatively impact the patients quality of life. To add further confusion the majority of trans-tibial sockets are based on conflicting principles, hands-on casting and pressure/hands-off casting. Hands-on casting relies

heavily on the prosthetist's skill, experience and beliefs [61]. As a result each cast is unique, are unable to be recreated and potentially highly inconsistent [19].

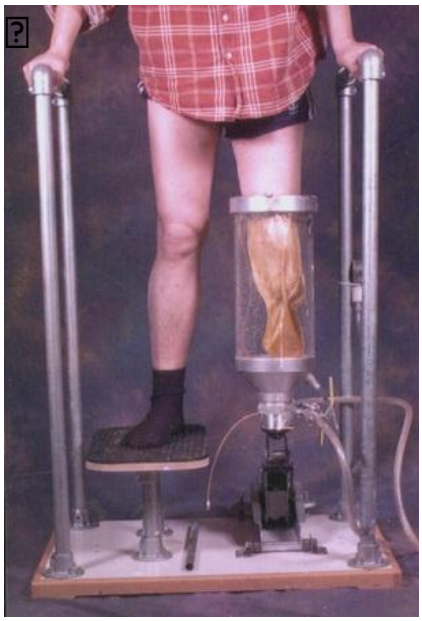

Figure 1.7 Controlled pressure casting

Buis et al [61]

Pressure casting (Figure 1.7) is based on placing the residual limb into a medium, such as water, creating uniform pressure similar to the loading of a prosthesis during gait, thus reducing human error [61]. Due to the lack of data on the internal mechanical conditions of the stump during weight-bearing [62] there is no consensus on optimal socket design or fit [15, 19]. Socket fit is dependent on a number of factors, one of which is the coupling stiffness or the mechanical stiffness of the connection between the rigid structure of the prosthesis and skeleton [19, 41]. Therefore the socket and soft tissue form part of the coupling mechanism, which is increasingly believed to be a major factor in optimising socket design [15, 19]. Enhanced stiffness is desired to reduce movement between the socket and skeleton, pistoning and increased proprioception [19, 63]. If there were a large degree of displacement between the skeleton and body of prosthesis this could lead to increased stump/socket interface, or frictional shear as well as internal shear [15, 19, 63]. Optimal coupling stiffness also reduces the risk of slippage, which is a factor in relative skeletal displacement to the socket [15]. This movement could lead to tissue deformation, which further increases the relative socket-skeleton displacement, thus increasing shear forces.

Further research evaluating the interface pressures, i.e. pressure between stump and socket, in isolation have inadequately quantify the mechanical stresses within deep internal tissues [2, 64]. Hence interfacial pressures alone are unlikely to change socket design principles and another factor is required for investigation.

1.5 Research Aim and Objectives

The aim of this project is to perform a feasibility study into whether shear stress does emit acoustic noise (specific noise frequency) in animal tissue, potentially in the 20Hz – 20kHz range during tensile testing. The objectives are:

1. Investigate suitable microphones for this signal.
2. Simultaneously record acoustic and deformation data during testing.
3. Develop and design a suitable experiment for testing and improve on previous work
4. Perform analysis on the data to determine characterisation of signal.

Due to the exploratory nature of this project what follows are a series of pilot test experiments which aim to find the optimum protocol

2 TEMPERATURE CONTROLLED TESTING

2.1 Methods

2.1.1 Specimens and Preparation

Baseline tests were performed on cotton fabric weave due to similarities in uni-directional fibres. Samples were harvested from two pork *psoas major* muscles, purchased from a local butcher's shop, into smaller segments. Bony attachments were avoided due to the failure of muscle rupture in previous work [20]. The *psoas major* muscle was selected due to the organised uni-directional nature of the fibres and ease of availability. The specimens were dissected when the muscle was frozen, however due to the initial freezing process the muscles were contorted and required to be thawed and refrozen into more easily dissectible fashion. From one muscle ten longitudinal specimens were dissected and the other ten transverse specimens (Figure 2.1). The specimens were thawed at room temperature prior to testing.

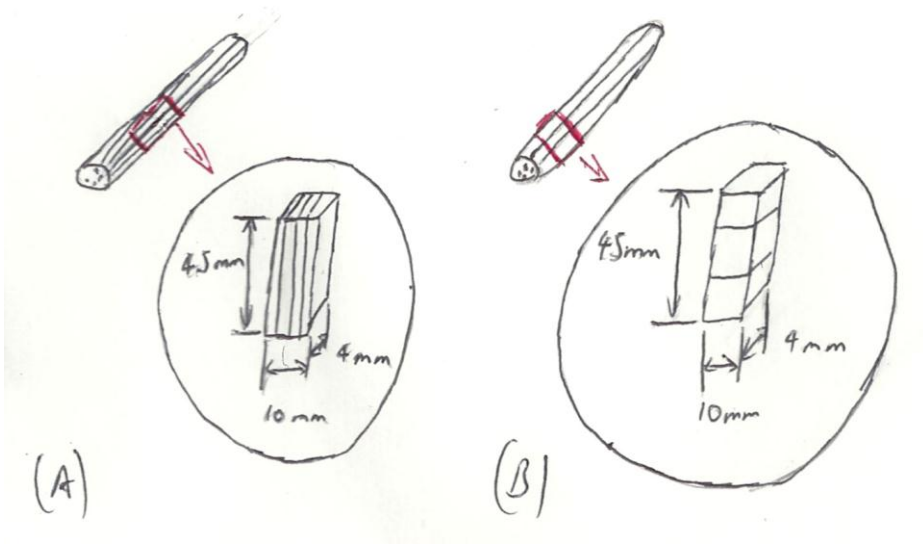

Figure 2.1 Harvesting test specimens

(A) displays how longitudinal fibres from the muscle were dissected into desired dimensions. (B) displays the transverse fibres

The tensile testing was performed with a 'Bose' or Electroforce® 3200 test instrument (Bose, USA) using a displacement control test. Due to the maximum displacement of the machine being 13mm, a target displacement of 10mm to fracture was decided. This formed the basis of specimen dimension calculation, shown in Appendix A, using a Young's Modulus of 0.4 MPa and fracture stress of 0.15 MPa [65] all specimens were roughly 45mm length, 10mm width and 4mm depth. The effective gauge length was 25mm, as the grips required 10mm of tissue. Therefore the calculated displacement for fracture, assuming a linear relationship, was just over 9mm, and a calculated fracture stress of 6N. Theoretically there could be AE during the elastic phase of the tissue, however it is uncertain where along this phase AE would occur hence specimen fracture was sought since it is visible and significant.

2.1.2 Equipment

The Bose machine was selected due to its superior sensitivity to displacement and load data in smaller specimens over the Instron machine used by Ralston, 2015 [20]. Specimens were clamped, using serrated grips, within a temperature controlled water bath of 37.2°C and a 450N submersible load cell was used (Figure 2.2). The

plain water bath allowed simulation of an *in vivo* environment as well as improved medium for the hydrophone.

An omni-directional hydrophone was utilised with a frequency range of 0.1Hz – 180kHz (Bruel and Kjaer Type 8103) with a voltage sensitivity of 30.0μV/Pa [66] and an inbuilt preamplifier. A digital oscilloscope (Tektronix DPO2014) was used to record hydrophone data directly from the oscilloscope display. This was done in real-time at a sampling frequency of 12.5kHz. Both Bose and hydrophone data were recorded simultaneously. Ralston [20] utilised a data synchronisation point by tapping the Instron load cell, however due to the delicate nature of the Bose load cell this was not possible, instead both programs were initiated simultaneously.

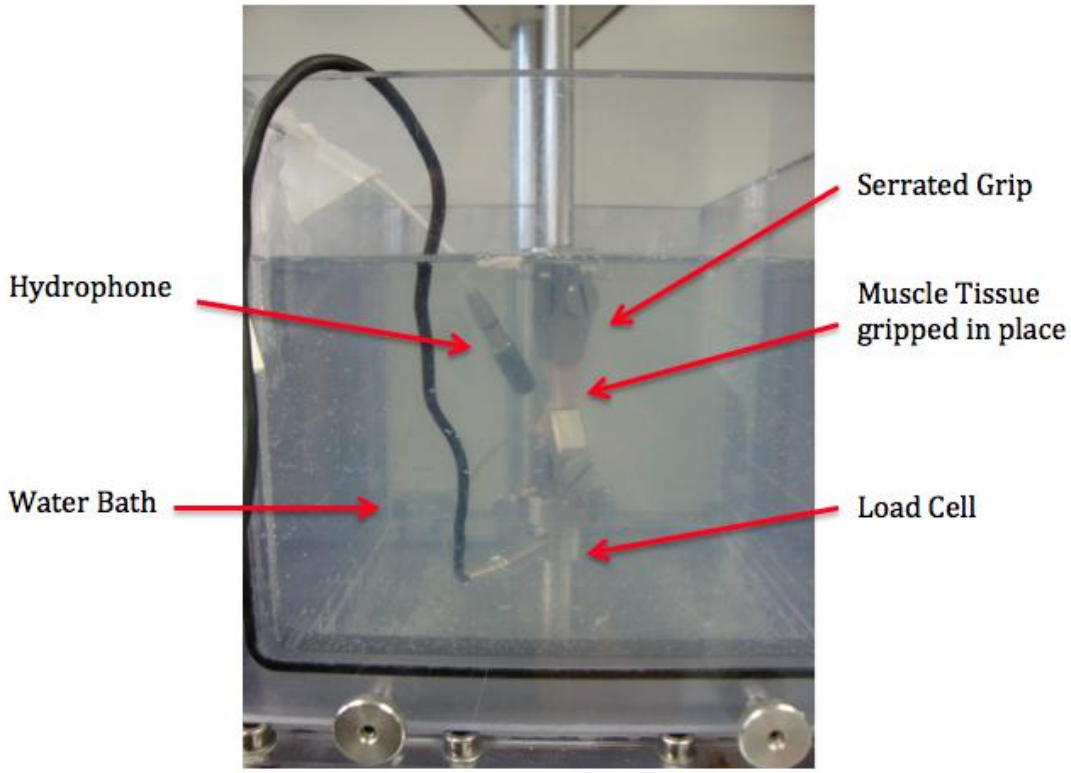

Figure 2.2 Bose Machine setup including water bath and hydrophone

2.1.3 Test Protocols

Two longitudinal specimens were subjected to tensile testing. There are a lack of publications available regarding the choices of tensile displacement rate as studies choose 1, 5 and 10mm/s for indentation testing with no justification [67, 68]. Due to previous calculations a maximum 9.5mm displacement at a rate of 1mm/sec was chosen. A slower strain rate was restricted by limited time for acoustic data collection from the oscilloscope display. Wintest 4.1™ software gathered time, displacement and load data at a sampling rate of 100Hz. This data was then exported to Microsoft Excel ™ for graphical representation. The time-domain acoustic data was then exported to MatLab ™ for further analysis. MatLab calculated the modulus of the Fourier transform for each time-domain signal to produce the frequency domain plot. This showed which frequencies were contained in the recorded time-domain data and the size of their contribution to the final signal. The Fast Fourier Transform algorithm in MatLab performed the discrete Fourier transform as the data was digitised. The discrete Fourier equation is shown below:

$$X(e^{j\omega}) = \sum_{n=-\infty}^{+\infty} x[n]e^{-j\omega n}$$

where ω is the angular frequency and n represents a finite number of samples of the complete recording. Finite in this case being between zero and infinite. Also the number of samples are integers i.e 1, 2, 3 as opposed to parts of numbers i.e. 1.2, 2.2, 3.2. The code for MatLab is shown in Appendix B.

2.2 Results

The baseline tests did not fracture due to the elasticity of the material and the limited displacement (13mm) of the Bose machine. The two specimens also did not visibly fail as the tests only placed the specimens in tension. The stress-strain curves of both tests are shown in Figure 2.3

There were no detectable acoustic signal when amplitude and time (time domain) where plotted of both tests. In the frequency domain (amplitude vs frequency) only noise was detected as seen in Figure 2.4.

s

2.3 Analysis and Method Modifications

The same issue occurred with the baseline fabric tests and tissue testing whereby further displacement was required to visibly acknowledge specimen failure. However it is interesting to see a peak in stress for Test 2 despite no fracture being visible. Two possibilities could provide an explanation; the first being that some fibres maybe fracturing but not visible to the eye. If this were plausible though then the stress should continue rising but at a different gradient, however, the curve is analogous to a specimen fracture. The second, more plausible, possibility could be the grip slipping and incomplete load transfer to the specimen. Either way due to safety limits, to prevent machine damage, visible specimen fracture could not be achieved.

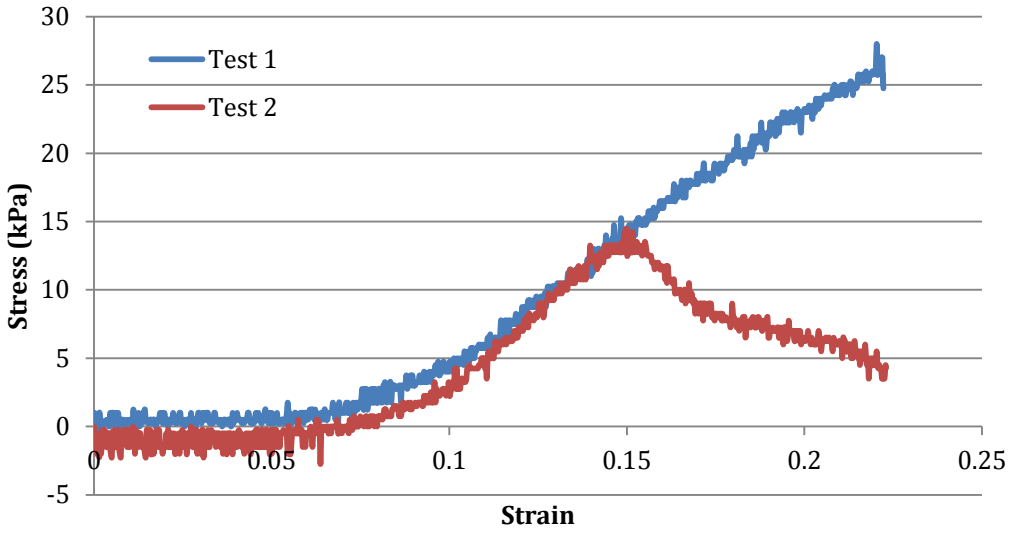

Figure 2.3 Stress-strain curves of two 45mm longitudinal specimens placed under 9mm displacement of uniaxial tension

It was also noted that once thawed the tissue was highly elastic and could stretch up to 55mm in length. Therefore further testing was performed with thawed specimens then crudely stretched and dissected at 45mm and 35mm at room temperature. These specimens both had longitudinal and transverse fibre orientation, however failure still could not be achieved.

An alternative could have been to place a fixed amount of tensile load prior to displacement so that the specimen would be taut. However programming the Bose machine to perform a load controlled phase would have been difficult due to the creep of the tissue i.e. slow tissue deformation under constant load, in this case tissue

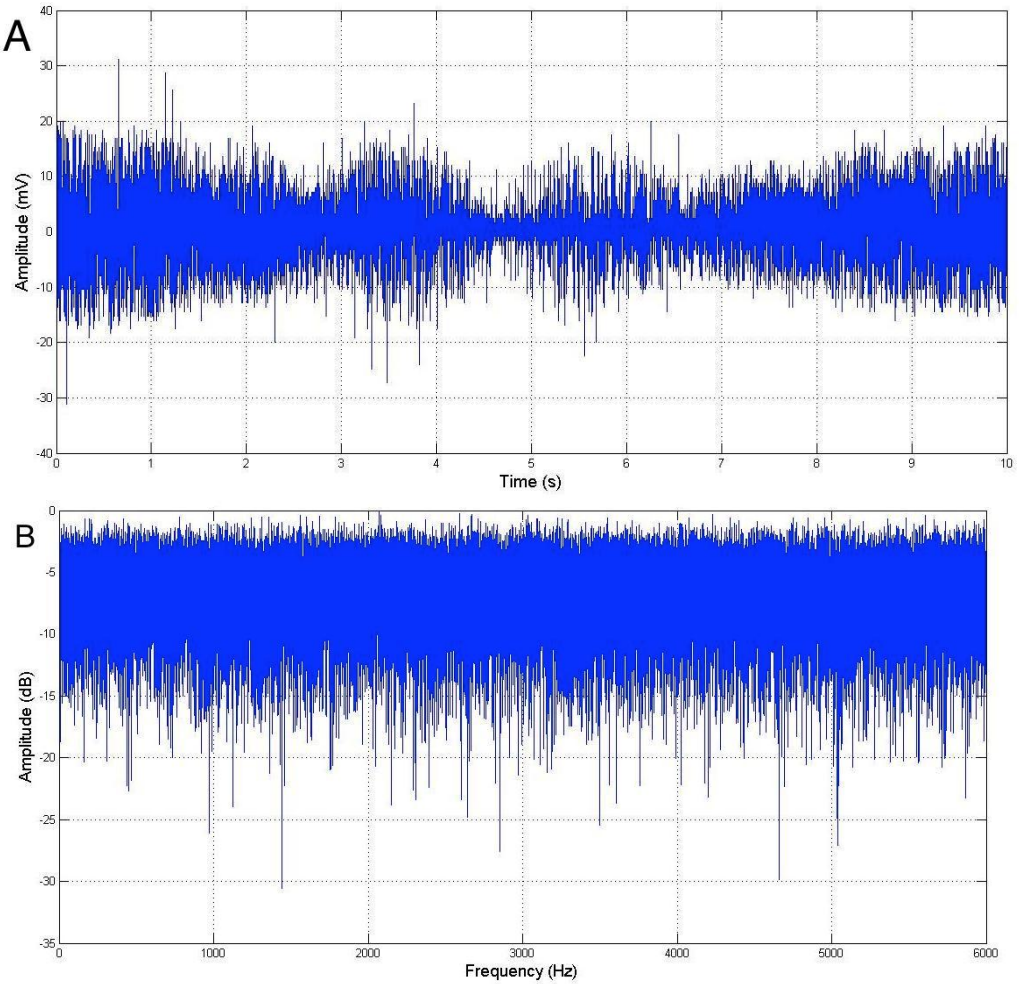

Figure 2.4 Time and Frequency plots of Test 2

Both tests exhibited the same trends in the time (A) and frequency (B) domain, using a logarithmic scale, hence only one test was displayed

elongation. Another challenge would be in determining the amount of load required.

Due to these challenges it was decided to further shorten the specimens for the next set of experiments to 25mm, total length. Whilst modifying the protocol all acoustic recording displayed the same amplitude plots as Figure 2.4. It was noted that a large amount of background noise was present and even palpable vibrations were

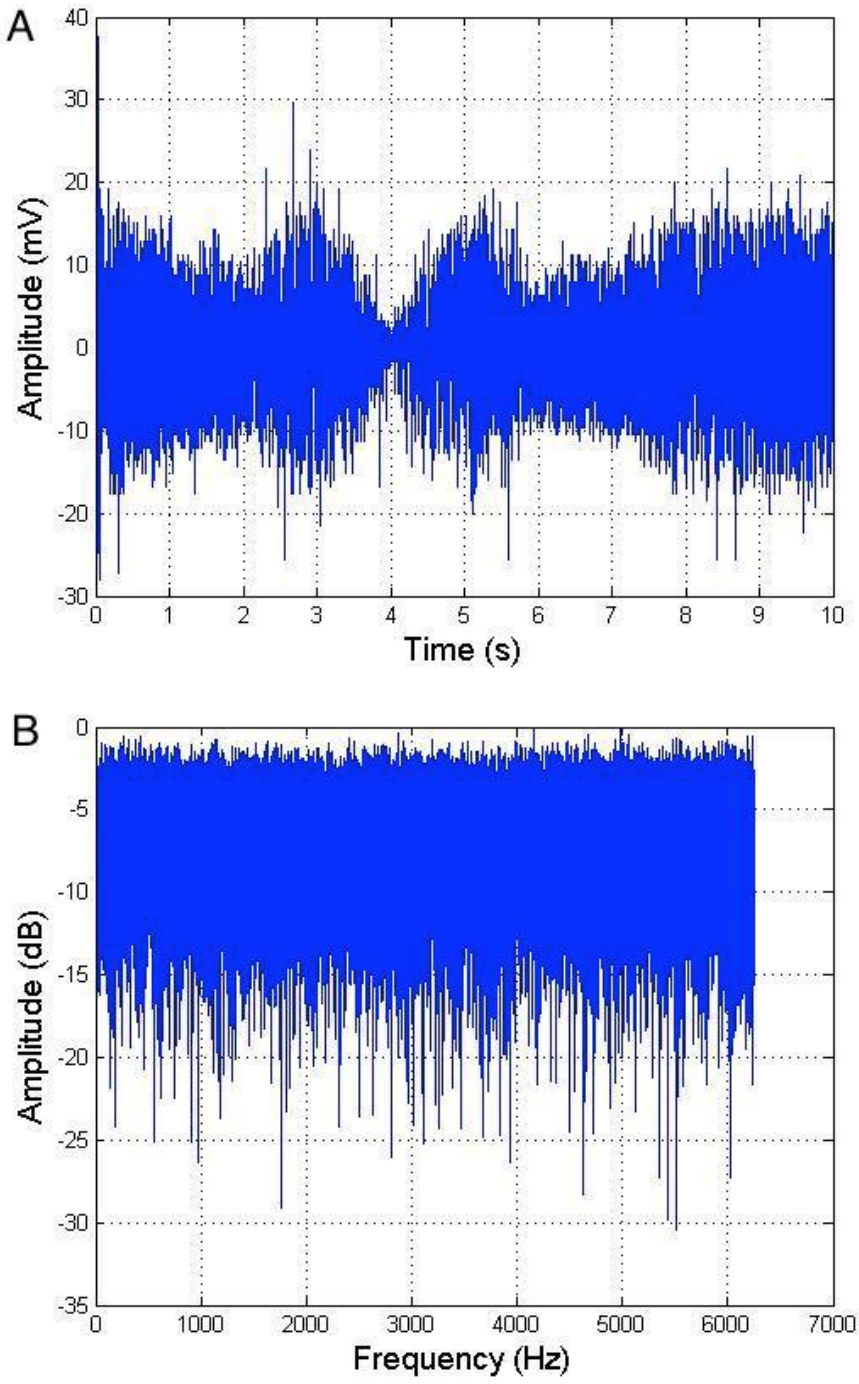

Figure 2.5 Time and Frequency domain plots of Bose machine noise

The acoustic recording was delayed by a second after the Bose machine had initiated displacement as seen in Figure 2.5a. The Frequency domain or power spectrum is displayed in Figure 2.5b with a logarithmic scale

detected on the water bath wall. To provide certainty that Figure 2.4a was due to machine noise a tensile test was performed with no specimen present. The time and frequency domain plots are displayed in Figure 2.5 which similar to Figure 2.4.

Figure 2.5 also highlighted the challenge of ensuring consistency in synchronised recording of acoustic and Bose data. A potential solution would be

using a computer interface to provide continuous acoustic recording or at least more accurate initiation such as Spike ^{TM} (Cambridge Electronic Design, Cambridge, UK) which is used in electromyography recording. Due to time pressures and uncertainty in signal characteristics this type of software was not utilised.

To reduce the amount of noise a non-temperature controlled bath was chosen for the next set of experiments. It also proved more beneficial for the tissue specimens as they were being effectively cooked thus changing their mechanical properties [69, 70].

3 NON-TEMPERATURE CONTROLLED TESTING

3.1 Methods

The remaining specimens were shortened, when frozen, to 25mm length, thus the effective gauge length shortened to 5mm. The other dimensions remained the same as in Figure 2.1. The specimens were placed into the same assembly as Figure 2.2, however the water bath had no temperature control. The hydrophone was consistently positioned roughly 1cm away from the tissue.

3.1.1 Test Protocols

Further calculations estimated tissue failure should occur approximately at 2mm (Appendix A), since strain rate was maintained at 1mm/s a 1s hold phase at zero displacement was introduced at the start. This was to allow for acoustic data to be recorded and not miss the failure event which occurred in some initial tests (not presented in this study). Two initial pilot tests (PL1 and PL2) were performed with transverse specimens to a maximum displacement of 7mm. For the remaining specimens maximum displacement was set at 9mm to ensure the best chance of specimen fracture. Four transverse (TR) and three longitudinal specimens (LO) were tested using the same recording software in section 2.1.3.

3.2 Results

PL1 and PL2 displayed partial failure whereby parts of the specimens had been torn. In PL1 an unusual cluster of amplitude was noted on the oscilloscope display, between the fifth and sixth second of recording (Figure 3.1a). However in the time domain plot this cluster was hardly noticeable (Figure 3.1b) due to machine noise. This noise was visible on the oscilloscope display, as a light background hue, but cannot be seen in Figure 3.1a. Unless one specifically focused on that time interval (Figure 3.2) then parts of the cluster can be seen. The time domain plot of PL2 resembled Figure 2.4a which was not included in this results section. Both frequency domain plots of PL1 and PL2 were the same as Figure 2.4b.

The stress-strain curves of PL1 and PL2 are displayed in Figure 3.3 and Figure 3.4 shows the nature of the partial fractures. PL1 appeared more disorganised whilst PL2 was more of a tear.

Of the four transverse specimens, two displayed complete failure (TR1 and TR3), one a partial tear (TR2) and the last showed a slight tear at the bottom grip (TR4). Though some acoustic data was noted on the oscilloscope display during recording, again the time and frequency domain plots resembled that of Figure 2.4 hence are not presented. When the stress-strain curves were plotted TR1 and TR2 seemed to have been mislabelled and have not been included in this section but are presented in Appendix C. The stress-strain curves of TR3 and TR4 are shown in Figure 3.5 whereby the failure stress of TR3 was roughly 10 kPa. One can also see the partial tear of TR4 occurred at 5 kPa.

During tensile testing of the three longitudinal specimens none failed and the stress-strain curves are displayed in Figure 3.6. Again the time and frequency domain plots resembled Figure 2.4 as relevant data on the oscilloscope display being lost to machine noise.

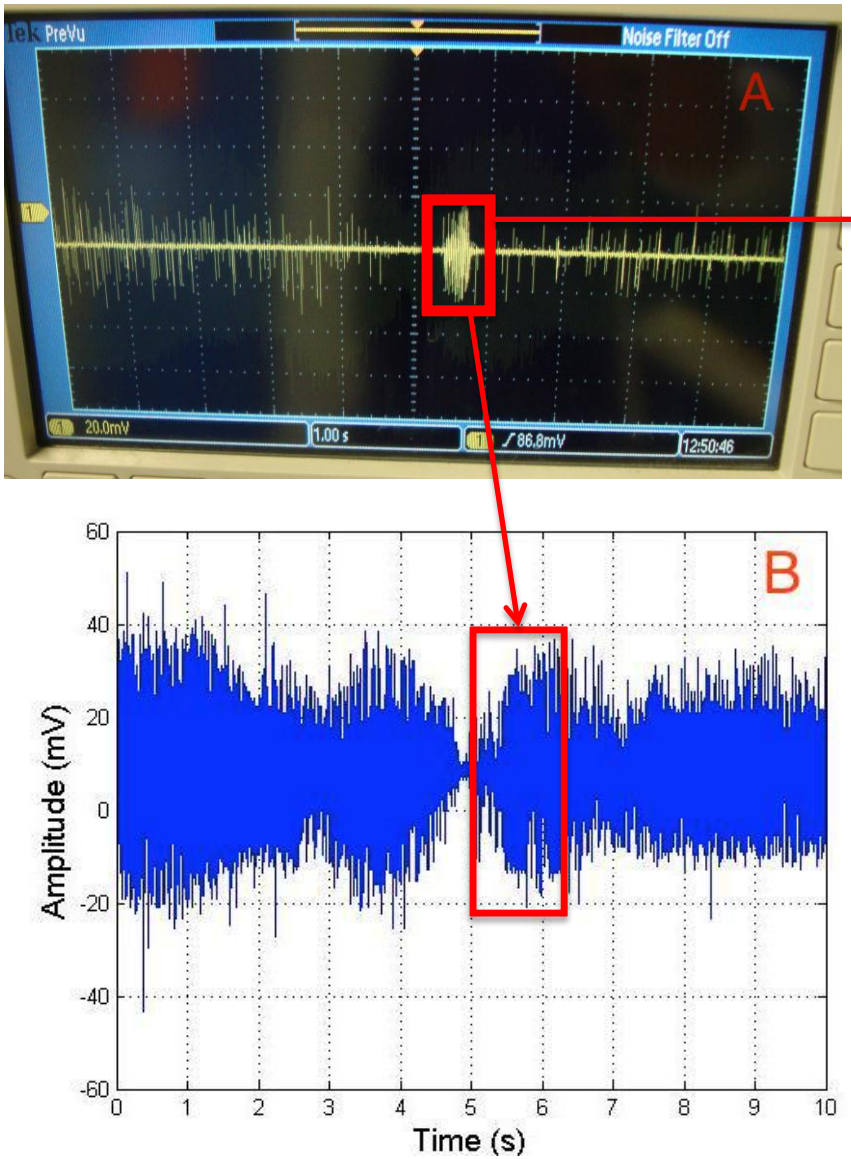

Figure 3.1 Oscilloscope display and time plot of PL1

(A) The oscilloscope display of PL1 where each horizontal interval represents 1s and (B) shows the time domain plot of the recording

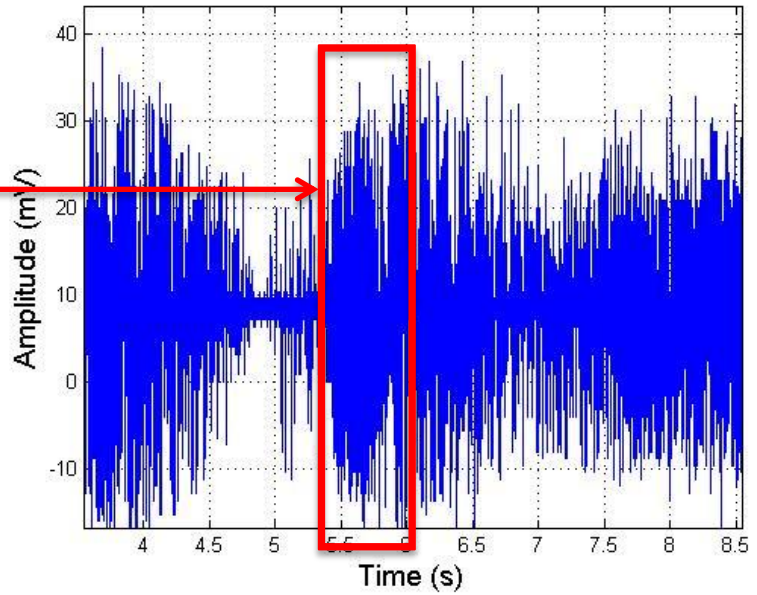

Figure 3.2 Zoomed in display of time domain plot for PL1

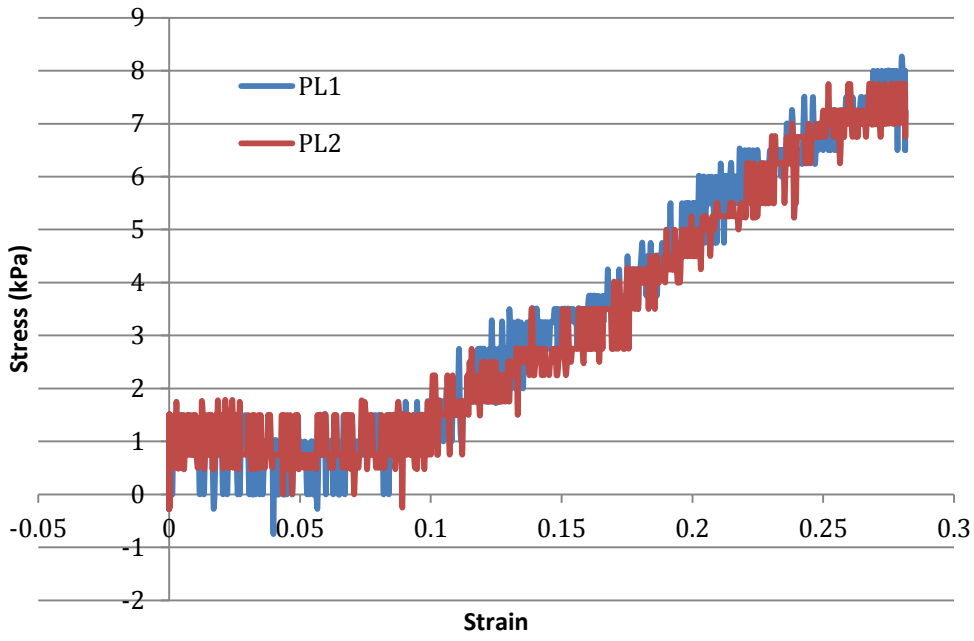

Figure 3.3 Stress-strain curves of PL1 and PL2

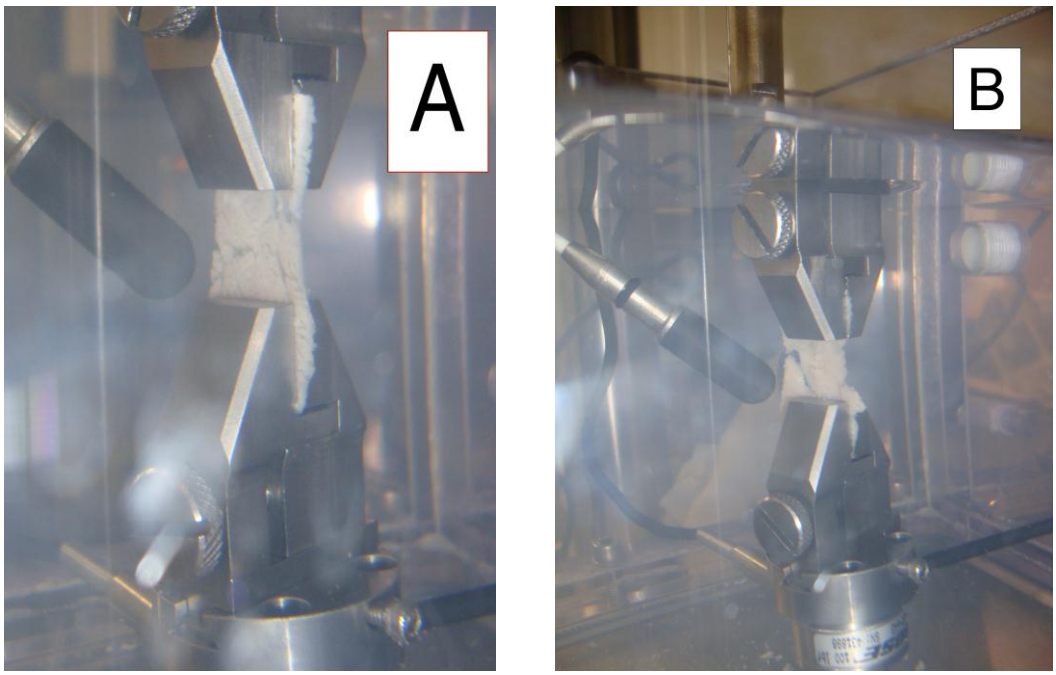

Figure 3.4 Displaying the nature of the PL1 and PL2 partial failure
PL1 on the left and PL2 on the right.

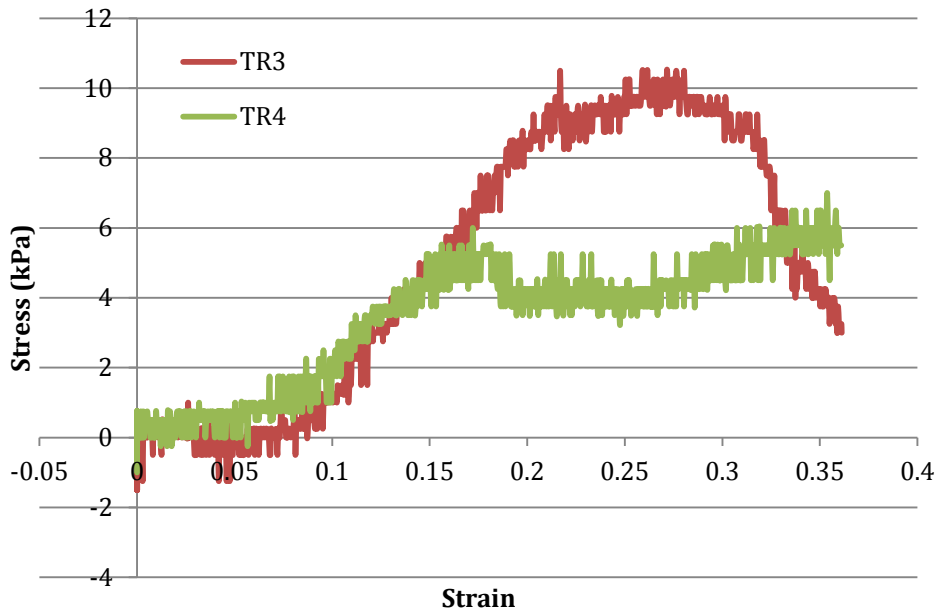

Figure 3.5 Stress-strain curves of transverse specimens

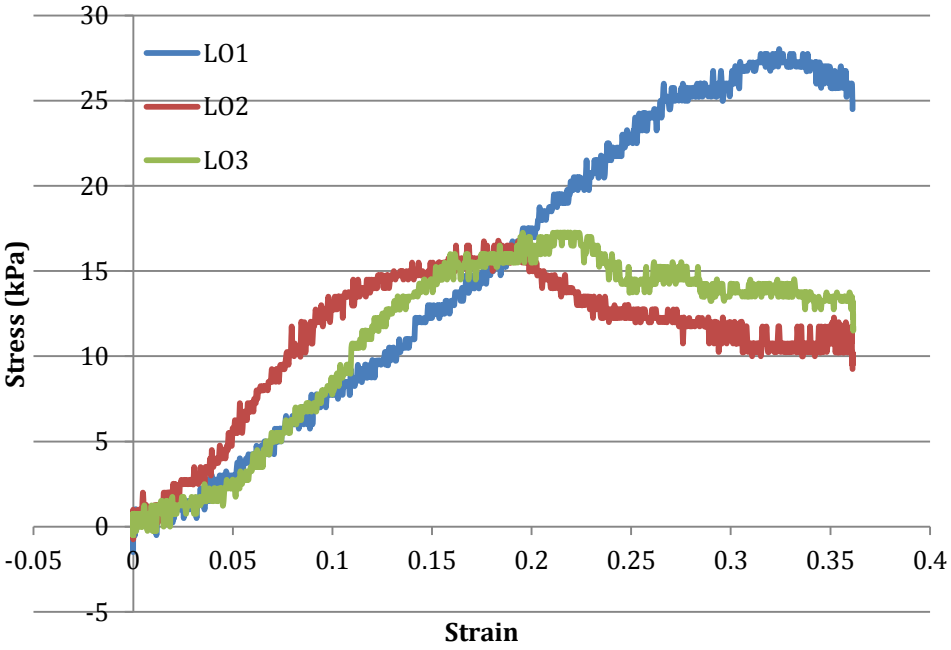

Figure 3.6 Stress-strain curves of longitudinal specimens

4 DISCUSSION

These experiments were conducted to investigate whether animal tissue emits acoustic noise under shear stress. Due to the small number of trials performed statistical analysis was not performed.

During testing the hydrophone did seem to detect possible acoustic noise of tissue deformation and failure (Figure 3.1a), however due to the large amount of environmental noise this has not been quantifiable or able to be utilised when analysed. The time domain plots of all specimens, regardless of whether failure was achieved, displayed the same general trend of noise from the Bose machine. This lead to all frequency plots being the same as Figure 2.4b.

There are several limitations with this study which are now discussed.

4.1 Acoustic Recording

The use of recording software such as Spike ™ and a data synchronisation point would have been beneficial. The main limitations of acoustic recording can be viewed as the instruments being too coarse and are discussed under four areas.

4.1.1 Noisy Environment

The Bose machine produced a large amount of noise during tensile testing (Figure 2.5) and attempts had been made to reduce this interference. However, the exclusion of the temperature controlled bath did little to exclude the noise. If the

tissue specimens were kept small then either a different tensile testing instrument would be required or the avoidance of water as the conducting medium. An alternative, as Ralston [20] had suggested, could be to use a contact microphone placed on to the tissue itself. However, due to the dimensions of such a transducer (20mm diameter) specimen failure would not be achieved in the current protocol, as seen in the temperature controlled testing. To gain further displacement to fracture these specimens one could use a linear actuator which provides a further 50mm displacement, however due to time constraints this was not utilised in these experiments.

In Ralston's experiments an Instron machine was utilised and there seemed to be little machine noise detected [20]. An alternative to the Bose machine could be to use whole fresh chicken thigh muscles without their bony attachment and place in the Instron machine for acoustic detection.

4.1.2 Louder Acoustic Sound

This leads into another viewpoint that the specimens were too quiet for acoustic signal production. To resolve this challenge larger, thicker specimens would be required however due to the viscoelastic nature of muscle [19, 71-73], specifically the elastic response, further displacement would be needed. It is also worthwhile to note that only transverse specimens failed and not longitudinal specimens. In the transverse orientation the main load-bearing element would be the connective tissue within skeletal muscle [74] and it is likely these connections between muscle fascicles and fibres were failing. If more displacement could be achieved then possibly longitudinal specimens will provide a louder acoustic signal, as actual muscle fibres would be fractured.

4.1.3 Microphone suitability

In this study a hydrophone was utilised to record acoustic data. Signal aliasing is unlikely due to a sampling frequency of 12.5 kHz and a maximum frequency response of 180 kHz. Hence Nyquist limit has not been reached. Whether this hydrophone was sensitive enough or had an appropriate frequency range to detect acoustic signals is uncertain as its intended use is for cavitations and

underwater animal calls. The AE may be at higher frequency than the acoustic range or too quiet for detection. The addition of a further preamplifier would only increase the machine noise in this current protocol. An alternative transducer would be a contact microphone however the Bose machine noise may counteract any advantage of the contact microphone. It would be useful, in the future, to test a range of microphones with differing characteristics to establish the most suitable one. For example this hydrophone was omni-directional meaning it is a non-directional transducer that is equally sensitive to sounds from all directions. If a uni-directional transducer was used this could potentially eliminate surrounding sounds and focus on a single point.

4.1.4 Signal to Noise Ratio

In order to increase the SNR (signal to noise ratio) a baseline of the environment would be required which was taken in Figure 2.5. This could theoretically be used to eliminate the noise in the recordings, however the feasibility of such method is uncertain. An alternative is to utilise a form of common mode rejection by constructing a differential amplifier similar to Barry and Cole [56] with two hydrophones. Upon further review of the literature tackling the issue of SNR would be important as the frequency of muscle contraction is very low, between 17-28 Hz [75]. More emphasis on signal processing would be required to increase the SNR to enable a utilisation for DTI detection.

4.2 Tensile Protocols and Data

Though a tensile loading protocol was performed this is not the same as shear, which has an important role in DTI development [21]. However, it has been assumed that internal shear stresses are present during tensile loading due to the induction of a pressure gradient [19, 63].

4.2.1 Displacement and Grips

In order to fracture more specimens, further displacement would be required than acheivable. Placing a pre-tension load may have provided a resolution but would have been technically challenging. There was a degree of grip slippage which

seems to be displayed in the peaks of stress-strain curves of LO1-LO3. Due to time pressures a more rigorous method of attaching the specimens to the grips of the Bose machine was not achievable. It also seems, when combining the tensile data from the two pilot tests (PL1 and PL2) with TR3 and TR4, the transverse specimens were less likely to slip than longitudinal specimens. This could be due the longitudinal specimens being stronger and able to withstand higher stresses than transverse specimens.

4.2.2 Tensile Data

Interestingly this is contrary to Nie et al [74] findings where they performed dynamic and quasi-static tensile loading on porcine muscle at different strain rates. They found transverse specimens were stronger which had higher deformation resistance and the perimysium, or the connective tissue sheaths surrounding muscle fibre bundles, was the main load-bearing element. They suggested the stretch-resistant characteristics were responsible for such findings. Nie et al did preserve their tissue in a modified Kreb solution to simulate the in vivo environment, which was not performed in this study. However Nie et al did not submerge their specimens in water during tensile testing. These two factors could explain why the transverse specimens proved to be weaker in this study.

4.2.3 Tissue Preparation

Ideally biological specimens should be prepared and tested within a few hours of death to preserve the mechanical properties. It has been documented that freezing muscle alters and reduces it strength [76]. In contrast Huang et al has documented that thawing then refreezing tendons less than 3 cycles does not significantly alter the mechanical properties [77]. Despite these conflicting findings biological tissue should be tested fresh if possible or preserved in a manner that reflects the in vivo environment with minimum freezing.

4.2.4 Strain Rate

Most biological tissues including skeletal muscle and connective tissue are described as viscoelastic in nature [19, 63, 71-73]. This means they exhibit both

viscous, i.e. fluid-like behaviour resisting shear, and elastic, i.e. rapidly returning to original state, characteristics when strained. Specifically with muscle it displays elasticity when it returns to its original shape when stretched then released [73]. It's viscosity is the internal resistance to motion [73]. As a result of this viscoelasticity time is also an important factor as viscosity dissipates the shear force [67, 78]. This is further corroborated by porcine muscle displaying different levels of stress to a variety of strain rates [74]. In amputees DTI is more likely to occur over long periods of cyclical gait motion in a multi-directional orientation. If it were possible to record acoustic data over a longer period of time then a slower more realistic strain rate could be employed along with compression testing to recreate forces experienced by the residual limb.

5 CONCLUSIONS AND FUTURE WORK

This study provides inconclusive evidence whether acoustic emission exists on tissue deformation. Tensile testing of transverse pork psoas major muscle fibres did produce deformation and failure, however due to the tensile testing instrumentation no acoustic signal was detectable. The large number of assumptions and limitations means these results cannot be extrapolated to the *in vivo* environment.

Moving forward more sensitive, quieter instruments should be sought which deforms longitudinal muscle fibres. Incorporation of a data synchronisation point, if possible, along with acoustic recording software would also increase accuracy. A larger number of preserved specimens, reflecting the *in vivo* environment, are required to perform statistical analysis.

6 REFERENCES

1. NPUAP, EPUP, PPIA. Prevention and Treatment of Pressure Ulcers: Quick Reference Guide. In: Haesler EE, editor. Perth, Australia: Cambridge Media; 2014.

2. Gefen A, Levine J. The false premise in measuring body- support interface pressures for preventing serious pressure ulcers. Journal of medical engineering & technology, 2007, Vol31(5), pp375-80.31(5).

3. Gefen A, Gefen N, Linder-Ganz E, Margulies SS. In vivo muscle stiffening under bone compression promotes deep pressure sores. Journal of biomechanical engineering 2005, Vol127(3), pp512-24.127(3).

4. NPUAP, EPUAP. Treatment of pressure ulcers: quick reference guide.: Washington DC: National Pressure Ulcer Advisory Panel; 2009.

5. Mak AFT, Yu Y, Kwan L, Sun L, Tam E. Deformation and reperfusion damages and their accumulation in subcutaneous tissues during loading and unloading: A theoretical modeling of deep tissue injuries. Journal Of Theoretical Biology, 2011 Nov 21, Vol289, pp65-73.289.

6. Stekelenburg A, Strijkers G, Parusel H, Bader DL, Nicolay K, Oomens CW. Role of ischemia and deformation in the onset of compression-induced deep tissue injury: MRI-based studies in a rat model. Journal Of Applied Physiology, 2007 May, Vol102(5), pp2002-2011.102(5).

7. Agam L, Gefen A. Pressure ulcers and deep tissue injury: a bioengineering perspective. Journal of wound care, September 2007, Vol16(8), pp336-342.16(8).

8. Bansal C, Scott R, Stewart D, Cockerell CJ. Decubitus ulcers: a review of the literature. International journal of dermatology 2005, Vol44(10), pp805-10.44(10).

9. Black J, Baharestani MM, Cuddigan J, Dorner B, Edsberg L, Langemo D, et al. National Pressure Ulcer Advisory Panel's updated pressure ulcer staging system. Advances in skin & wound care, May 2007, Vol20(5), pp269-74.20(5).

10. Linder-Ganz E, Gefen A. Mechanical compression-induced pressure sores in rat hindlimb: muscle stiffness, histology, and computational models. Journal of Applied Physiology. 2004;96(6):2034-49.

11. Bouten CV, Oomens CW, Baaijens FP, Bader DL. The etiology of pressure ulcers: Skin deep or muscle bound? Archives of Physical Medicine and Rehabilitation. 2003;84(4):616-9.

12. Black JM. Moving toward consensus on deep tissue injury and pressure ulcer staging. Advances in skin & wound care. 2005;18(8):415-6, 8, 20-21.

13. Ephraim PL, Dillingham TR, Sector M, Pezzin LE, MacKenzie EJ. Epidemiology of limb loss and congenital limb deficiency: A review of the literature. Archives of Physical Medicine and Rehabilitation. 2003;84(5):747-61.

14. Lago N, Navarro X. Evaluation of the long-term regenerative potential in an experimental nerve amputee model. Journal of the Peripheral Nervous System. 2007;12(2):108-20.

15. Mak AFT, Zhang M, Boone DA. State-of-the-art research in lower-limb prosthetic biomechanics-socket interface: A review. Journal of Rehabilitation Research and Development, 2001, Vol38(2), pp161-173.38(2).

16. Ceelen KK, Stekelenburg A, Loerakker S, Strijkers GJ, Bader DL, Nicolay K, et al. Compression-induced damage and internal tissue strains are related. Journal of Biomechanics. 2008;41(16):3399-404.

17. Stekelenburg A, Gawlitta D, Bader DL, Oomens CW. Deep Tissue Injury: How Deep is Our Understanding? Archives of Physical Medicine and Rehabilitation, 2008, Vol89(7), pp1410-1413.89(7).

18. Portnoy S, Gefen I, Siev-Ner N, Kristal A, Shabshin Z, Yizhar A. Patient-specific analyses of deep tissue loads post transtibial amputation in residual limbs of multiple prosthetic users. Journal of Biomechanics, 11 December 2009, Vol42(16), pp2686-2693.42(16).

19. Klasson B, Buis, AWP. Prosthetic Socket Fit; Implications of basic engineering principles. 94 912 Advanced prosthetic science (manual 3): NCPO, University of Strathclyde, Glasgow; 2006.

20. Ralston Z. Acoustic emission, detection and analysis of tissue deformation: a feasibility study: Thesis [B. Sc. Prosthetics and Orthotics] -- University of Strathclyde; 2015.

21. Gefen A, Farid K, Shaywitz I. A Review of Deep Tissue Injury Development, Detection, and Prevention: Shear Savvy. Ostomy Wound Management, 2013 Feb, Vol59(2), pp26-35.59(2).

22. Gefen A. Risk factors for a pressure-related deep tissue injury: a theoretical model. Medical & Biological Engineering & Computing, 2007, Vol45(6), pp563-573.45(6).

23. Farid K, Farid M, Andrews CM. Total contact casting as part of an adaptive care approach: a case study. Ostomy/wound management 2008, Vol54(6), pp50-65.54(6).

24. Institute NC. SEER Training:Structure of Skeletal Muscle. 2015 [04/08/2015]; Available from: http://training.seer.cancer.gov/anatomy/muscular/structure.html.

25. Levine J. RHABDOMYOLYSIS IN ASSOCIATION WITH ACUTE PRESSURE SORE. Journal Of The American Geriatrics Society, 1993 Aug, Vol41(8), pp870-872.41(8).

26. Linder-Ganz E, Shabshin N, Gefen A. Patient-specific modeling of deep tissue injury biomechanics in an unconscious patient who developed myonecrosis after prolonged lying. Journal of Tissue Viability, 2009, Vol18(3), pp62-71.18(3).

27. Makhsous M, Lin F, Pandya A, Pandya MS, Chadwick C. Elevation in the Serum and Urine Concentration of Injury-Related Molecules After the Formation of Deep Tissue Injury in a Rat Spinal Cord Injury Pressure Ulcer Model. Pm&R, 2010 Nov, Vol2(11), pp1063-1065.2(11).

28. Bagley W, Yang H, Shah K. Rhabdomyolysis. Internal and Emergency Medicine, 2007, Vol2(3), pp210-218.2(3).

29. Gefen A. How Much Time Does it Take to Get a Pressure Ulcer? Integrated Evidence from Human, Animal, and In Vitro Studies. Ostomy Wound Management, 2008 Oct, Vol54(10), pp26-+.54(10).

30. Levitov A, Mayo P, A S. Critical Care Ultrasonography. New York, NY: The McGraw-Hill Companies, Inc; 2009.

31. Anesthesia UfR. Generation of an Ultrasound Image. 2008 [updated 04/08/2015]; Available from: http://www.usra.ca/generationofimage.php.

32. Rumack CM, Wilson SR, Charboneau JW, D L. Diagnostic Ultrasound, Vol. 2. Philadelphia, PA: Elsevier, Mosby; 2011. 2 – 52 p.

33. Deprez J-F, Brusseau E, Fromageau J, Cloutier G, Basset O. On the potential of ultrasound elastography for pressure ulcer early detection. Medical Physics. 2011;38(4):1943-50.

34. Hansen GL, Sparrow EM, Kommamuri N, Iaizzo PA. Assessing wound severity with color and infrared imaging of reactive hyperemia. Wound repair and regeneration : official publication of the Wound Healing Society [and] the European Tissue Repair Society, 1996, Vol4(3), pp386-92.4(3).

35. Moghimi S, Miran Baygi MH, Torkaman G, Mahloojifar A. Quantitative assessment of pressure sore generation and healing through numerical analysis of high-frequency ultrasound images. Journal of rehabilitation research and development, 2010, Vol47(2), pp99-108.47(2).

36. Farid K. Applying observations from forensic science to understanding the development of pressure ulcers. Ostomy Wound Management, 2007 Apr, Vol53(4), pp26-+.53(4).

37. Iaizzo PA. Temperature modulation of pressure ulcer formation: Using a swine model. Wounds, November 2004, Vol16(11), pp336-343.16(11).

38. Harder Y, Amon M, Georgi M, Erni D, Menger MD. Evolution of a 'falx lunatica' in the demarcation of critically ischemic myocutaneous tissue. Journal Of Vascular Research, 2004, Vol41(5), pp465-465.41(5).

39. Steeds RP, Alexander PJ, Muthusamy R, Bradley M. Sonography in the diagnosis of rhabdomyolysis. Journal of clinical ultrasound : JCU, 1999, Vol27(9), pp531-3.27(9).

40. Aoi N, Yoshimura K, Kadono T, Nakagami G, Iizuka S, Higashino T, et al. Ultrasound Assessment of Deep Tissue Injury in Pressure Ulcers: Possible Prediction of Pressure Ulcer Progression. Plastic And Reconstructive Surgery, 2009 Aug, Vol124(2), pp540-550.124(2).

41. Murray K, Convery P. The calibration of ultrasound transducers used to monitor motion of the residual femur within a trans- femoral socket during gait. Prosthetics And Orthotics International, 2000 Apr, Vol24(1), pp55-62.24(1).

42. Berger A. Magnetic resonance imaging. BMJ : British Medical Journal. 2002;324(7328):35-.

43. Fleckenstein JL. Skeletal muscle evaluated by MRI. In: Grant DM, Harris, R.K., editor. Encyclopedia of Nuclear Magnetic Resonance. Chichester: Wiley; 1996. p. 4430-6.

44. van Nierop BJ, Stekelenburg A, Loerakker S, Oomens CW, Bader D, Strijkers GJ, et al. Diffusion of water in skeletal muscle tissue is not influenced by compression in a rat model of deep tissue injury. Journal of Biomechanics, 2010, Vol43(3), pp570-575.43(3).

45. Alger JR. The Diffusion Tensor Imaging Toolbox. The Journal of Neuroscience. 2012;32(22):7418-28.

46. Huang M, Jiang L, PK L, CR B, DL K. Using Acoustic Emssion in Fatigue and Fracture Materials Research. Journal of Materials, Metals and Minerals society [Internet]. 1998; 50(11). Available from: http://www.tms.org/pubs/journals/JOM/9811/Huang/Huang-9811.html.

47. Joselin R, Chelladurai T. Burst Pressure Prediction of Composite Pressure Chambers Using Acoustic Emission Technique: A Review. Journal of Failure Analysis and Prevention, 2011, Vol11(4), pp344-356.11(4).

48. Kohn DH. Acoustic emissions and non- destructive evaluation of biomaterials and tissues. Critical Reviews in Biomedical Engineering, 1995, Vol23(3-4), pp221-306.23(3-4).

49. Williams RV. Acoustic emission. Bristol: Bristol Hilger; 1980.

50. I.M. T. Acoustic emission as a technique for monitoring failure within vertebral bodies: Thesis [M. Sc.] -- University of Strathclyde, 1986.

51. Ralston Z, Guarato F, Buis A. Acoustic emission, detection and analysis of tissue deformation: a feasibility study: Thesis [B. Sc. Prosthetics and Orthotics] -- University of Strathclyde; 2015.

52. Stokes M, Dalton PA. ACOUSTIC MYOGRAPHY FOR INVESTIGATING HUMAN SKELETAL-MUSCLE FATIGUE. Journal Of Applied Physiology, 1991 Oct, Vol71(4), pp1422-1426.71(4).

53. Islam A, Sundaraj K, Ahmad B, Ahamed N, Ali A. Mechanomyography Sensors for Muscle Assessment: a Brief Review.

54. Barry DT, Geiringer SR, Ball RD. Acoustic myography: a noninvasive monitor of motor unit fatigue. Muscle & nerve, 1985, Vol8(3), pp189-94.8(3).

55. Barry DT, Leonard JA, Gitter AJ, Ball RD. Acoustic myography as a control signal for an externally powered prosthesis. Archives of physical medicine and rehabilitation, April 1986, Vol67(4), pp267-9.67(4).

56. Barry D, Cole N. MUSCLE SOUNDS ARE EMITTED AT THE RESONANT FREQUENCIES OF SKELETAL- MUSCLE. Ieee Transactions On Biomedical Engineering, 1990 May, Vol37(5), pp525-531.37(5).

57. Frangioni JV, Kwan-Gett TS, Dobrunz LE, McMahon TA. The mechanism of low- frequency sound production in muscle. Biophysical Journal, 1987, Vol51(5), pp775-783.51(5).

58. Buis A, McGarry A, Gachagan A, Riches P. Acoustic emission, detection and analysis of deep tissue injury (DTI) in trans-tibial prosthetic sockets (Research Proposal). University of Strathclyde: AOPA; 2011.

59. Buis A, McGarry A, Gachagan A, Riches P. Acoustic emission, detection and analysis of deep tissue injury (DTI) in trans-tibial prosthetic sockets (Research Proposal). 2011.

60. Stewart C. Synopsis of Causation, Lower Limb Amputation. Ministry of Defence, 2008.

61. Buis A, McGarry A, Gachagan A, Riches P. Acoustic emission, detection and analysis of deep tissue injury (DTI) in trans-tibial prosthetic sockets (Draft Research Proposal - File name 'Shear Noise Project'). 2011.

62. Portnoy S, Yizhar Z, Shabshin N, Itzchak Y, Kristal A, Dotan-Marom Y, et al. Internal mechanical conditions in the soft tissues of a residual limb of a trans-tibial amputee. Journal of Biomechanics, 2008, Vol41(9), pp1897-1909.41(9).

63. Klasson B. Appreciation of prosthetic socket fitting from basic engineering principles. Services RI, editor. Glasgow (GB): Glasgow GB : National Centre for Training and Education in Prosthetics and Orthotics; 1995.

64. Yarnitzky G, Yizhar Z, Gefen A. Real-time subject-specific monitoring of internal deformations and stresses in the soft tissues of the foot: A new approach in gait analysis. Journal of Biomechanics, 2006, Vol39(14), pp2673-2689.39(14).

65. Taylor D, O'Mara N, Ryan E, Takaza M, Simms C. The fracture toughness of soft tissues. Journal of the Mechanical Behavior of Biomedical Materials. 2012;6:139-47.

66. Kjær b. Miniature hydrophone with integral 6m cable terminated 10-32UNF microdot plug. 2015 [21/08/2015]; Available from: http://www.bksv.com/Products/transducers/acoustic/hydrophones/8103?tab=overview.

67. Silver-Thom MB. In vivo indentation of lower extremity limb soft tissues. IEEE Transactions on Rehabilitation Engineering, September 1999, Vol7(3), pp268-277.7(3).

68. Tonuk E, Silver-Thorn MB. Nonlinear elastic material property estimation of lower extremity residual limb tissues. Ieee Transactions On Neural Systems And Rehabilitation Engineering, 2003 Mar, Vol11(1), pp43-53.11(1).

69. Mutungi G, Purslow P, Warkup C. Structural and mechanical changes in raw and cooked single porcine muscle fibres extended to fracture. Meat Science, 1995, Vol40(2), pp217-234.40(2).

70. Willems MET, Purslow PP. Mechanical and structural characteristics of single muscle fibres and fibre groups from raw and cooked pork longissimus muscle. Meat Science, 1997, Vol46(3), pp285-301.46(3).

71. Crawford SK, Haas C, Wang Q, Zhang X, Zhao Y, Best TM. Effects of immediate vs. delayed massage-like loading on skeletal muscle viscoelastic properties following eccentric exercise. Clinical Biomechanics.

72. Lieber RL, Leonard ME, Brown-Maupin CG. Effects of Muscle Contraction on the Load- Strain Properties of Frog Aponeurosis and Tendon. Cells Tissues Organs, 2000, Vol166(1), p48-54.166(1).

73. Nihat Oz. Fundamentals of biomechanics : equilibrium, motion, and deformation. Margareta N, editor. New York: New York : Springer; 1999.

74. Nie X, Cheng J, Chen W, Weerasooriya T. Dynamic Tensile Response of Porcine Muscle. Journal Of Applied Mechanics-Transactions Of The Asme, 2011 Mar, Vol78(2).78(2).

75. Ouamer M, Boiteux M, Petitjean M, Travens L, Salès A. Acoustic myography during voluntary isometric contraction reveals non-propagative lateral vibration. Journal of biomechanics 1999, Vol32(12), pp1279-85.32(12).

76. Gottsauner-Wolf F, Grabowski JJ, Chao EY, An KN. Effects of freeze/thaw conditioning on the tensile properties and failure mode of bone-muscle- bone units: a biomechanical and histological study in dogs. Journal of orthopaedic research : official publication of the Orthopaedic Research Society 1995, Vol13(1), pp90-5.13(1).

77. Huang H, Zhang J, Sun K, Zhang X, Tian S. Effects of repetitive multiple freeze-thaw cycles on the biomechanical properties of human flexor digitorum superficialis and flexor pollicis longus tendons. Clinical biomechanics (Bristol, Avon), May 2011, Vol26(4), pp419-23.26(4).

78. Christensen RM. Theory of viscoelasticity : an introduction. New York: New York : Academic Press; 1971.

7 APPENDICES

Appendix A – Specimen Dimension Calculation

Stress (σ) = Force (F)/Area (A) Young's Modulus (E) = Stress (σ)/ Strain (ε)

Strain = Change in Length (ΔL)/ Original Length (L)

For Pork muscle:

E = 0.4 MPa and Fracture Stress (σ_F) = 0.15 MPa

$\varepsilon = \sigma_F/E$ = 0.15/0.4 = 0.375

A = 4mm x 10mm = 0.004m x 0.01m = 4×10^{-5} m^2

ΔL>10mm $\Delta L = L \times \varepsilon$

Temperature controlled Tests:

Gauge Length = 45mm ∴ $\Delta L = 25 \times 0.375 = 9.375$mm

$F = \sigma \times A$ ∴ Fracture Load (F) = (1.5×10^5 Pa) x (4×10^{-5} m^2) = 6 N

Non-temperature controlled testing:

Gauge Length = 5mm ∴ $\Delta L = 5 \times 0.375 = 1.875$mm

Appendix B – MatLab Code for Acoustic Data Analysis.

```
close all
clear all
clc

M = csvread('T0004CH1.CSV', 32, 0);
% M = csvread('T0002CH1.CSV', 32, 0); % only noise
time = M(:, 1)+ 5;

sig = (M(:, 2)-M(1, 2))*1000; %+0.0384;
Ts = time(6) - time(5);
Fs = 1/Ts;

figure;
plot(time, sig)
xlabel ('Time (s)', 'FontSize', 14)
ylabel ('Amplitude (mV)', 'FontSize', 14)
grid on

SIG = abs(fft(sig));
LF = (Fs/2) * linspace(0, 1, length(SIG(1:floor(length(SIG)/2))));

x_min = 0;
x_max = 2500;
y_min = 0;
y_max = 5;

figure;
plot(LF, SIG(1:floor(length(SIG)/2)))
xlabel ('Frequency (Hz)', 'FontSize', 14)
ylabel ('Amplitude', 'FontSize', 14)
axis([x_min x_max y_min y_max])
grid on

% Divide by max value and logaritmic scale
SIG_dB = zeros(1, floor(length(SIG)/2));
for i = 2:floor(length(SIG)/2)
    SIG_dB(i) = 10*log10(SIG(i) / max(SIG(2:floor(length(SIG)/2))));
end

figure;
plot(LF, SIG_dB)
xlabel ('Frequency (Hz)', 'FontSize', 14)
ylabel ('Amplitude (dB)', 'FontSize', 14)
% axis([x_min x_max y2_min y2_max])
grid on
```

Appendix C – Stress-Strain Curves of TR1 – TR3

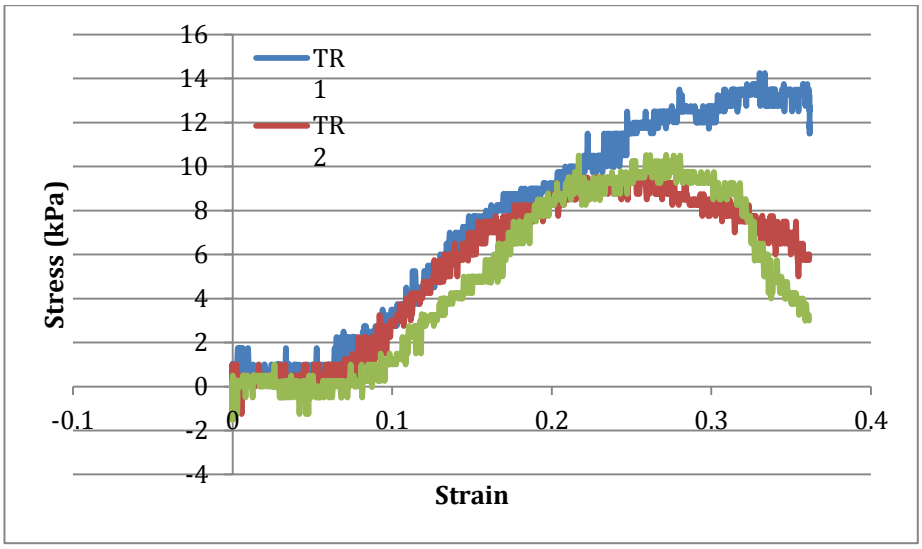

The curves for TR1 – TR3. It was noted that TR1 and TR3 sustained complete fracture and TR2 a partial fracture. TR3 displayed a typical failure curve which is corroborated by another stress-strain curve, below, of a transverse specimen which sustained complete fracture. This was not presented in the study.

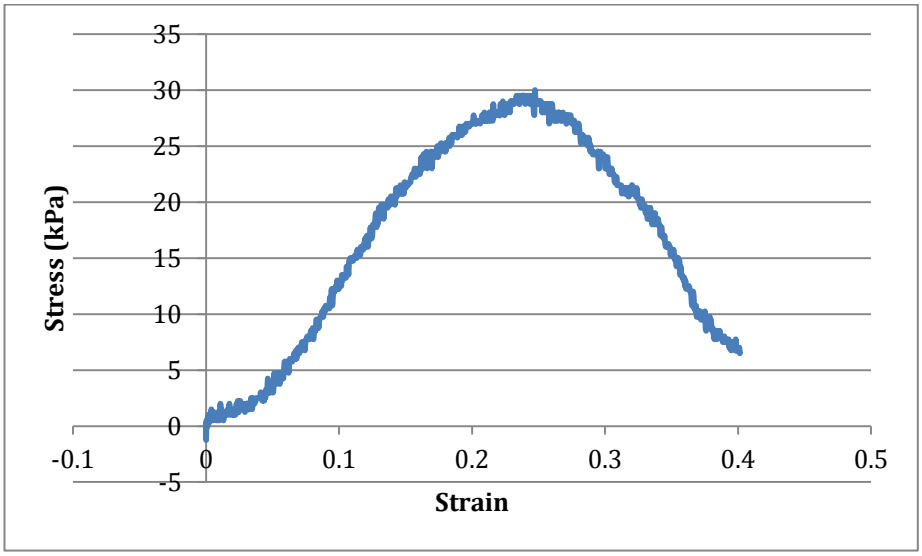

TR2, which was noted as a partial fracture, had a curve more similar with TR3 and the above non-presented specimen. If a partial fracture was sustained then the stress-strain curve should not have a clear peak and possibly continue to increase like the curve TR1. If TR1 was a complete fracture then a peak stress should be present. Due to these discrepancies TR1 and TR2 were not included as it seemed more likely that mislabelling had occurred.

Appendix D – Data of PL1

A sample of the Acoustic Data. Only the first hundred data points are included here.

TIME	CH1	CH1 Peak Detect
-5.00E+00	-0.0356	0.0164
-5.00E+00	-0.014	-0.046
-5.00E+00	-0.014	0.0172
-5.00E+00	-0.0148	-0.062
-5.00E+00	-0.014	0.0316
-5.00E+00	-0.014	-0.0708
-5.00E+00	-0.014	0.042
-5.00E+00	-0.0132	-0.074
-5.00E+00	-0.0148	0.0452
-5.00E+00	-0.0148	-0.0604
-5.00E+00	-0.014	0.0276
-5.00E+00	-0.014	-0.0468
-5.00E+00	-0.0148	0.018
-5.00E+00	-0.0132	-0.046
-5.00E+00	-0.014	0.0188
-5.00E+00	-0.014	-0.0452
-5.00E+00	-0.0228	0.0156
-5.00E+00	-0.0148	-0.05
-5.00E+00	-0.0132	0.0204
-5.00E+00	-0.014	-0.0492
-5.00E+00	-0.014	0.0196
-5.00E+00	-0.014	-0.0468
-5.00E+00	-0.014	0.0172
-5.00E+00	-0.0148	-0.046
-5.00E+00	-0.0212	0.0164
-5.00E+00	-0.0148	-0.0452
-5.00E+00	-0.0036	0.0164
-5.00E+00	-0.0148	-0.0444
-5.00E+00	-0.014	0.0156
-5.00E+00	-0.0148	-0.046
-5.00E+00	-0.0148	0.0172
-5.00E+00	-0.014	-0.0476
-5.00E+00	-0.0004	0.0172
-5.00E+00	-0.0156	-0.0452
-5.00E+00	-0.0148	0.0156
-5.00E+00	-0.026	-0.046
-5.00E+00	-0.0148	0.0164

-5.00E+00	-0.0148	-0.0452
-5.00E+00	-0.0148	0.0164
-5.00E+00	-0.014	-0.0452
-5.00E+00	-0.0388	0.0164
-5.00E+00	-0.014	-0.046
-5.00E+00	-0.014	0.0164
-5.00E+00	-0.014	-0.0444
-5.00E+00	-0.0148	0.0156
-5.00E+00	-0.014	-0.0452
-5.00E+00	-0.0148	0.0156
-5.00E+00	-0.014	-0.0484
-5.00E+00	-0.0148	0.0172
-5.00E+00	-0.0132	-0.05
-5.00E+00	-0.014	0.018
-5.00E+00	-0.0132	-0.0452
-5.00E+00	-0.0004	0.0164
-5.00E+00	-0.014	-0.046
-5.00E+00	-0.014	0.0156
-5.00E+00	-0.014	-0.0476
-5.00E+00	-0.018	0.0172
-5.00E+00	-0.0148	-0.046
-5.00E+00	-0.0148	0.0164
-5.00E+00	-0.014	-0.046
-5.00E+00	-0.0132	0.018
-5.00E+00	-0.018	-0.046
-5.00E+00	-0.014	0.0172
-4.99E+00	-0.014	-0.0476
-4.99E+00	-0.0148	0.0172
-4.99E+00	-0.014	-0.0468
-4.99E+00	-0.014	0.0172
-4.99E+00	-0.0156	-0.0452
-4.99E+00	-0.0148	0.0164
-4.99E+00	-0.014	-0.0452
-4.99E+00	-0.014	0.0164
-4.99E+00	-0.0148	-0.0484
-4.99E+00	-0.014	0.018
-4.99E+00	-0.014	-0.05
-4.99E+00	-0.0148	0.0212
-4.99E+00	-0.0148	-0.0492
-4.99E+00	-0.014	0.0204
-4.99E+00	-0.014	-0.0452
-4.99E+00	-0.0108	0.0172

-4.99E+00	-0.0156	-0.046
-4.99E+00	-0.0132	0.018
-4.99E+00	-0.014	-0.046
-4.99E+00	-0.0156	0.0164
-4.99E+00	-0.0156	-0.0468

The first 150 Tensile data points of PL1

Points	Elapsed Time	Scan Time	Disp	Load 2 Sbm
	Sec	Sec	mm	N
1	0	0	-5.032	-0.73
2	0.01	0.01	-5.032	-0.73
3	0.02	0.02	-5.032	-0.7
4	0.03	0.03	-5.032	-0.73
5	0.04	0.04	-5.033	-0.69
6	0.05	0.05	-5.033	-0.73
7	0.06	0.06	-5.033	-0.73
8	0.07	0.07	-5.032	-0.7
9	0.08	0.08	-5.033	-0.7
10	0.09	0.09	-5.032	-0.73
11	0.1	0.1	-5.032	-0.74
12	0.11	0.11	-5.032	-0.69
13	0.12	0.12	-5.032	-0.7
14	0.13	0.13	-5.033	-0.7
15	0.14	0.14	-5.033	-0.7
16	0.15	0.15	-5.033	-0.7
17	0.16	0.16	-5.032	-0.7
18	0.17	0.17	-5.032	-0.7
19	0.18	0.18	-5.032	-0.7
20	0.19	0.19	-5.032	-0.7
21	0.2	0.2	-5.033	-0.73
22	0.21	0.21	-5.032	-0.73
23	0.22	0.22	-5.032	-0.73
24	0.23	0.23	-5.031	-0.7
25	0.24	0.24	-5.032	-0.73
26	0.25	0.25	-5.032	-0.73
27	0.26	0.26	-5.032	-0.7
28	0.27	0.27	-5.031	-0.73
29	0.28	0.28	-5.031	-0.7
30	0.29	0.29	-5.031	-0.7
31	0.3	0.3	-5.032	-0.73

32	0.31	0.31	-5.031	-0.74
33	0.32	0.32	-5.031	-0.73
34	0.33	0.33	-5.031	-0.73
35	0.34	0.34	-5.032	-0.69
36	0.35	0.35	-5.031	-0.7
37	0.36	0.36	-5.031	-0.7
38	0.37	0.37	-5.031	-0.73
39	0.38	0.38	-5.032	-0.69
40	0.39	0.39	-5.031	-0.73
41	0.4	0.4	-5.032	-0.69
42	0.41	0.41	-5.032	-0.7
43	0.42	0.42	-5.031	-0.73
44	0.43	0.43	-5.031	-0.73
45	0.44	0.44	-5.033	-0.73
46	0.45	0.45	-5.032	-0.73
47	0.46	0.46	-5.032	-0.7
48	0.47	0.47	-5.032	-0.74
49	0.48	0.48	-5.032	-0.7
50	0.49	0.49	-5.032	-0.73
51	0.5	0.5	-5.032	-0.73
52	0.51	0.51	-5.032	-0.73
53	0.52	0.52	-5.032	-0.69
54	0.53	0.53	-5.033	-0.73
55	0.54	0.54	-5.032	-0.69
56	0.55	0.55	-5.031	-0.74
57	0.56	0.56	-5.031	-0.7
58	0.57	0.57	-5.032	-0.73
59	0.58	0.58	-5.032	-0.69
60	0.59	0.59	-5.032	-0.73
61	0.6	0.6	-5.031	-0.69
62	0.61	0.61	-5.031	-0.7
63	0.62	0.62	-5.032	-0.69
64	0.63	0.63	-5.031	-0.73
65	0.64	0.64	-5.032	-0.73
66	0.65	0.65	-5.032	-0.73
67	0.66	0.66	-5.032	-0.7
68	0.67	0.67	-5.032	-0.73
69	0.68	0.68	-5.032	-0.7
70	0.69	0.69	-5.032	-0.7
71	0.7	0.7	-5.032	-0.7
72	0.71	0.71	-5.032	-0.7

73	0.72	0.72	-5.032	-0.69
74	0.73	0.73	-5.032	-0.7
75	0.74	0.74	-5.033	-0.73
76	0.75	0.75	-5.032	-0.73
77	0.76	0.76	-5.032	-0.73
78	0.77	0.77	-5.032	-0.7
79	0.78	0.78	-5.032	-0.73
80	0.79	0.79	-5.032	-0.7
81	0.8	0.8	-5.032	-0.74
82	0.81	0.81	-5.032	-0.73
83	0.82	0.82	-5.032	-0.7
84	0.83	0.83	-5.032	-0.73
85	0.84	0.84	-5.033	-0.7
86	0.85	0.85	-5.032	-0.73
87	0.86	0.86	-5.031	-0.7
88	0.87	0.87	-5.032	-0.7
89	0.88	0.88	-5.032	-0.73
90	0.89	0.89	-5.031	-0.69
91	0.9	0.9	-5.031	-0.73
92	0.91	0.91	-5.032	-0.73
93	0.92	0.92	-5.032	-0.7
94	0.93	0.93	-5.032	-0.73
95	0.94	0.94	-5.032	-0.74
96	0.95	0.95	-5.031	-0.7
97	0.96	0.96	-5.032	-0.67
98	0.97	0.97	-5.032	-0.73
99	0.98	0.98	-5.032	-0.7
100	0.99	0.99	-5.032	-0.73
1	0.9998	0	-5.032	-0.69
2	1.0098	0.01	-5.032	-0.73
3	1.0198	0.02	-5.028	-0.73
4	1.0298	0.03	-5.02	-0.69
5	1.0398	0.04	-5.011	-0.73
6	1.0498	0.05	-5.001	-0.73
7	1.0598	0.06	-4.993	-0.69
8	1.0698	0.07	-4.981	-0.7
9	1.0798	0.08	-4.973	-0.69
10	1.0898	0.09	-4.962	-0.7
11	1.0998	0.1	-4.952	-0.69
12	1.1098	0.11	-4.943	-0.69
13	1.1198	0.12	-4.933	-0.69

14	1.1298	0.13	-4.922	-0.67
15	1.1398	0.14	-4.912	-0.69
16	1.1498	0.15	-4.902	-0.7
17	1.1598	0.16	-4.892	-0.67
18	1.1698	0.17	-4.881	-0.69
19	1.1798	0.18	-4.872	-0.69
20	1.1898	0.19	-4.861	-0.7
21	1.1998	0.2	-4.852	-0.69
22	1.2098	0.21	-4.84	-0.67
23	1.2198	0.22	-4.832	-0.69
24	1.2298	0.23	-4.82	-0.69
25	1.2398	0.24	-4.81	-0.69
26	1.2498	0.25	-4.801	-0.69
27	1.2598	0.26	-4.79	-0.67
28	1.2698	0.27	-4.78	-0.69
29	1.2798	0.28	-4.77	-0.69
30	1.2898	0.29	-4.76	-0.69
31	1.2998	0.3	-4.75	-0.7
32	1.3098	0.31	-4.74	-0.73
33	1.3198	0.32	-4.73	-0.69
34	1.3298	0.33	-4.72	-0.7
35	1.3398	0.34	-4.709	-0.7
36	1.3498	0.35	-4.7	-0.73
37	1.3598	0.36	-4.689	-0.7
38	1.3698	0.37	-4.679	-0.7
39	1.3798	0.38	-4.669	-0.69
40	1.3898	0.39	-4.66	-0.7
41	1.3998	0.4	-4.649	-0.69
42	1.4098	0.41	-4.639	-0.7
43	1.4198	0.42	-4.63	-0.69
44	1.4298	0.43	-4.619	-0.7
45	1.4398	0.44	-4.608	-0.74
46	1.4498	0.45	-4.598	-0.73
47	1.4598	0.46	-4.589	-0.7
48	1.4698	0.47	-4.579	-0.7
49	1.4798	0.48	-4.568	-0.69
50	1.4898	0.49	-4.558	-0.7